CHALMERS
UNIVERSITY OF TECHNOLOGY

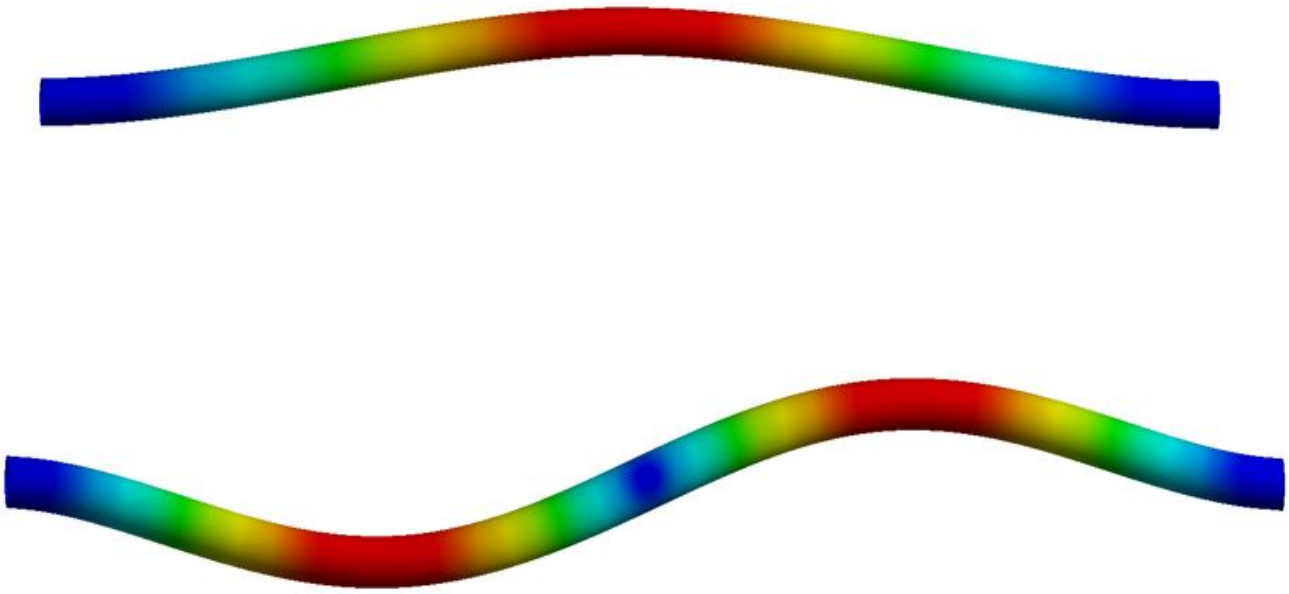

Methods for evaluating allowable vibration velocity levels in power plant piping systems

Master's thesis in Applied Mechanics

Marcus Ringström
Björn Wallin

Department of Mechanics and Maritime Sciences
CHALMERS UNIVERSITY OF TECHNOLOGY
Gothenburg, Sweden

MASTER'S THESIS IN APPLIED MECHANICS

Methods for evaluating allowable vibration velocity levels in power plant piping systems

Marcus Ringström
Björn Wallin

Department of Mechanics and Maritime Sciences
Division of Dynamics

CHALMERS UNIVERSITY OF TECHNOLOGY
Gothenburg, Sweden

Methods for evaluating allowable vibration velocity levels in power plant piping systems

Marcus Ringström
Björn Wallin

Master's Thesis 2019:107
Department of Mechanics and Maritime Sciences
Division of Dynamics
Chalmers University of Technology
SE-412 96 Gothenburg
Sweden
Telephone: + 46 (0)31-772 1000

Cover:
First and second bending mode for computational model 1.
Department of Mechanics and Maritime Sciences
Göteborg, Sweden

Methods for evaluating allowable vibration velocity levels in power plant piping systems

Master's thesis in Applied Mechanics
Marcus Ringström
Björn Wallin
Department of Mechanics and Maritime Sciences
Division of Dynamics
Chalmers University of Technology

Abstract

Vibrations in piping systems can have detrimental effects on the structural integrity, it is therefore of great importance to quantify the source of vibrations and to assess the impact of vibration induced fatigue. This thesis is limited to describe vibrations in a vibrating structure and not to investigate sources of excitation. The finite element method was used to perform modal synthesis and synthesis on three computational models with different levels of complexity. Modal analysis was performed by mode superposition which is an effective method used to approximate the dynamic response of a structure by superposition a small number of the structures eigenmodes.

The main objectives in this thesis are to investigate allowable vibration velocity levels for different methods. Allowable vibration velocity levels are determined by fatigue stress data obtained from fatigue curves. The endurance limit is taken as the fatigue stress at infinite lifetime, i.e. the stress where the material does not undergo fatigue. The endurance stress is thus set as the allowable limit for vibration velocities. Natural frequencies, modal displacement and modal stresses are obtained from the dynamic response from FE-analysis. Modal analysis was performed on all models and frequency response analysis with a prescribed acceleration amplitude has been performed on the most complex computational model to obtain vibration displacement and stress amplitudes, as well as forcing frequencies. The results show that all methods show the same trend for allowable vibration velocity with the only difference being allowable vibration velocity is shifted in magnitude for different methods. The first model exhibits a clear linear frequency dependence for allowable vibration velocity while model 2 and model 3 exhibit a more non-linear behaviour with respect to allowable vibration velocity due to combinations of vibrating modes.

Acknowledgements

We would like to thank John Lorentzon from Ringhals and Hans Tolke from Uniso for your support and dedication throughout this thesis. A special thanks to Uniso Technologies AB for giving us the opportunity to make this thesis. We would also like to thank our examiner Thomas Abrahamsson for useful input.

Marcus Ringström & Björn Wallin, Gothenburg, December 2019

Contents

Notations

Roman upper case letters

A, B	Integration constants, amplitude ratio
ASME	American Society for Mechanical Engineers
ASME OM	ASME Operations & Maintenance
ASME BPVC	ASME Boiler and Pressure Vessel Code
C_1	Correction factor that compensate the effects of concentrated weights
C_2K_2	Stress indices
C_3	Correction factor accounting for insulation and pipe content
C_4	Correction factor for different piping configurations
C_5	Correction factor to be used when the measured frequency differs from the first eigenfrequency of the piping span
D_0	Outer pipe diameter $[m]$
DOF	Degree-of-freedom
DMF_{ss}	Steady state dynamic magnification factor
E	Modulus of elasticity $\left[{}^{N}/_{m^2}\right]$
F_x	External force in x-direction $[N]$
FE-analysis	Finite Element analysis
$F(t)$	Driving force as a function of time $[N]$
$H(\alpha)$	Forcing frequency function
I	Moment of inertia $[m^4]$
I,J	Node I and J
$\boldsymbol{K}$	Stiffness matrix
K	Bulk modulus
L	Pipe length $[m]$
M	Mass of pipe $[kg]$
$\boldsymbol{M}$	Mass matrix
$M_{b,max,j}$	Maximum bending moment at mode j $[Nm]$
MDOF	Multiple degrees-of-freedom
$N_{eigenmodes}$	Number of eigenmodes
ODE	Ordinary differential equation
R	Stress ratio $[-]$
RMS	Root mean square
S	Nominal stress $[MPa]$
S_a	Allowable alternating peak stress $[MPa]$
S_{alt}	Maximum alternating stress intensity $[MPa]$
SDOF	Single degree-of-freedom
T	Time for one period $[s]$
V_{pipe}	Pipe volume $[m^3]$
VDI	Verein Deutscher Ingenieur
W	Pipe weight per unit length $\left[{}^{kg}/_{m}\right]$
W_f	Fluid weight per unit length $\left[{}^{kg}/_{m}\right]$
W_{INS}	Insulation weight per unit length $\left[{}^{kg}/_{m}\right]$
Z	Section modulus $[MPa]$

D	Scaled amplitude $[m]$
D_0	Static displacement $[m]$

Roman lower case letters

f_n	System natural frequency at mode n $[Hz]$
f_s	Spring force $[N]$
m	Mass $[kg]$
$\hat{m}_{eff,i,j}$	Effective mass at nth mode in the direction of j
m_{tot}	Total mass of the system
x	Displacement in x-direction $[m]$
$\boldsymbol{x}$	Position vector as a function of time
$\dot{\boldsymbol{x}}$	Velocity vector as a function of time
$\ddot{\boldsymbol{x}}$	Acceleration vector as a function of time
x_0	Initial displacement in x-direction $[m]$
x_p	Particular solution
$\ddot{x}$	Acceleration $\left[{}^{m}/_{s^2}\right]$
v,$\dot{x}$	Velocity $[{}^{m}/_{s}]$
ν	Poisson's ratio $[-]$
v_0	Initial velocity $[{}^{m}/_{s}]$
k	Spring constant $\left[{}^{N}/_{m}\right]$
k_{rot}	Rotational spring stiffness constant $\left[{}^{Nm}/_{deg}\right]$
max	Peak amplitude value
m_{med}	Mass of medium $[kg]$
n	Mode number
i	Imaginary number, $i = \sqrt{-1}$, stress index
r_a	External pipe radius $[m]$
$\boldsymbol{r}_j$	Mass displacement vector in the excitation direction j
$s_{1,2}$	Roots of characteristic equation
t	Time $[s]$
$u(x)$	Static deflection $[m]$
z	Complex number

Greek lower case letters

α	Ratio between forcing- and natural frequency [–]
β	Coefficient of thermal expansion $[K^{-1}]$
$\boldsymbol{\eta}$	Mode shape vector
δ_z	Rotation around z-axis
μ	Shear modulus $[Pa]$, mass loading $[kg/m]$
Δ	Peak amplitude value
ρ_{pipe}	Density of the pipe $[kg/m^3]$
ρ_{med}	Density of the medium $[kg/m^3]$
λ_{ij}	Modal participation factor at mode i in the excitation direction of j
$\boldsymbol{\rho}$	Complex vector containing all displacement amplitudes
$\Delta\sigma_R$	Stress range $[MPa]$
$\Delta\sigma_L$	Cut-off limit $[MPa]$
$\Delta\sigma_c$	Detail category $[MPa]$
$\Delta\sigma_D$	Constant amplitude fatigue limit $[MPa]$
σ	Elastic stress $[MPa]$
σ_m	Mean stress $[MPa]$
σ_a	Amplitude stress $[MPa]$
ϕ	Phase shift $[deg]$
ω_n	Natural frequency $[Hz]$
ω	Forcing frequency, angular frequency $[Hz]$

Miscellaneous symbols

$\bar{}$	Average
$\forall$	For all

1 Introduction

1.1 Background

All mechanical process systems are more or less subjected to some form of dynamic mechanical loading. Presence of dynamic mechanical loads will always generate vibrations in a mechanical system. The vibrations can be of transient character or of a stationary nature depending on the type of dynamic load. To determine the sources of unwanted vibrations for prevention purposes can be complex. Vibrations in power plants should be kept below allowable vibration velocity limits since it compromises the robustness of the plant, as it can lead to dangerous noise levels and fatigue failure. It is thus important to accurately quantify vibration levels and implement appropriate measures to avoid reaching dangerously high levels of vibrations both for economic reasons but also for safety reasons. In nuclear power plant industry, allowable vibration levels are often given as vibration velocity (Energiforsk 451, 2017, p.47).

In cases where vibrations are unavoidable it is important to have methods available to accurately quantify and evaluate vibration problems in a suitable way.

For example, in nuclear power plants continuous measurements are carried out to detect anomalies in vibration levels. If the source behind the vibration anomaly cannot be found, further measurements and evaluations are needed. Before the measurements can be carried out, an approximation is needed on which pipes and what frequency range to measure (Energiforsk 451, 2017, p.46). Modal analysis and harmonic response analysis could therefore be implemented to determine which objects and what frequency range to measure.

Pipe vibrations can be induced by several factors such as vortex induced vibrations which are amplified when vortex shedding frequencies matches the natural frequency of the structure. This fluid-structure interaction could lead to dangerous levels of vibration and ultimately component failure (VDI3842, 2004, p.11).

Vibrations can be divided in two groups: free vibrations and forced vibrations.
In free vibrations there are no external forces acting on the system. Motion is primarily the result of non-zero conditions, for example initial velocity or initial displacement of a mass element from an equilibrium position in a mass-spring system. Free vibrations of an elastic body are called natural vibrations, in this state the body is oscillating with its natural frequency. Examples of elastic forces could be restoring forces from a beam or a spring. Forced vibrations refers to the response of a structure when applying external loading. If the loading varies sinusoidally in time, the response is known as harmonic excitation (Ahmed A.S, 2019, pp. 2-3). The excitation can be induced by an applied force or a prescribed motion of the structure that support the system, for instance a prescribed acceleration amplitude.

The occurring vibration levels are heavily influenced by the amount of energy dissipated in a material through various damping forces such as viscous damping and/or structural damping. In vibration systems damping can be modelled by damping forcing functions that are proportional to velocity.

1.2 Aim

The aim of this thesis is to investigate different industrial methods to determine allowable pipe vibration velocity levels. In this context an allowable vibration velocity level is the velocity level acceptable in the piping system for fatigue failure, specifically high cycle fatigue induced by bending stress. The aim of the thesis also includes explaining and quantifying eventual differences between the methods and if possible, propose a preferred method to use.

1.3 Limitations

The systems simulated are undamped and excited by harmonic oscillation, where the effect of vibrations is studied and not how they are generated. Weld joints are limited to as-welded butt girth weld. The harmonic response analysis is limited to modal superposition. Fracture mechanics and fatigue life estimation models is not in the scope of this thesis and will thus not be included.

1.4 Scope

The methods studied in this thesis are:

- ASME OM-2015 / ASME BPVC 2015
- SS-EN-13445
- VDI 3842 / KTA 3211
- IIW 1823

Each code present design fatigue curves to determine an allowable lifetime in the form of number of load cycles. The amplitude stress for an infinite number of cycles, the endurance limit can be used for calculating an allowable vibration velocity. The methods are compared for three geometries with increasing complexity from a straight fixed-fixed pipe to a longer series of pipe sections containing spring supports.

2 Theory

2.1 Free Undamped Systems

The natural frequency of an object is a function of its mass and geometrical properties. The simplest example is the undamped SDOF system where an object with mass, m, is attached to a massless spring with spring constant, k. A frictionless mass-spring system is depicted in Figure 2.1.

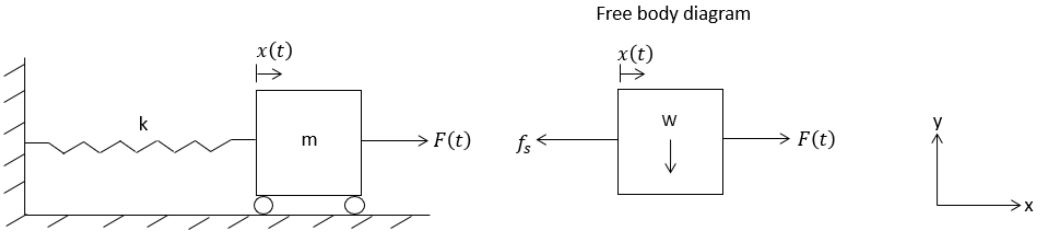

Figure 2.1- Undamped SDOF mass-spring system

Newtons second law on the system can be formulated as (Ahmed, A.S, 2019, p. 70-72):

$$\sum F_x = m\ddot{x} \rightarrow f_s + F(t) = m\ddot{x} \tag{1}$$

Where f_s is the spring force defined as:

$$f_s = -kx \tag{2}$$

The minus sign in equation (2) denote the force acting in the negative x-direction, $\ddot{x}$ denote acceleration of the system. $F(t)$ is the driving force as a function of time, k is the spring stiffness, x is an arbitrary position from its static equilibrium position and m is the mass of the object. For an undamped system in free vibration there is no external excitation and no external forces are acting on the system, i.e. $F(t) = 0$. A homogenous second order ODE can now be formulated for the system:

$$m\ddot{x} + kx = 0 \rightarrow \ddot{x} + \frac{k}{m}x = 0 \tag{3}$$

From equation (3), the system natural frequency, f, and angular natural frequency, ω_n is given by the following relations:

$$\omega_n = \sqrt{\frac{k}{m}}, \qquad f = \frac{\omega_n}{2\pi} = \frac{1}{2\pi}\sqrt{\frac{k}{m}} \tag{4}$$

By inserting equation (4) in equation (3), the ODE can now be defined as:

$$\ddot{x} + \omega_n^2 x = 0 \tag{5}$$

The general solution to equation (5) is obtained from the initial conditions, $x(t=0) = x_0$ and $\dot{x}(t=0) = v_0$, where x_0 and v_0 are initial displacement and velocity respectively. The general solution for Equation (6) have the form:

$$x(t) = Ae^{i\omega_n t} + Be^{-i\omega_n t} \tag{6}$$

If A and B are complex integration constants, equation (6) can be simplified as:

$$x(t) = \frac{X}{2}\left(e^{i(\omega_n t - \phi)} + e^{-i(\omega_n t - \phi)}\right) = X\cos(\omega_n t - \phi) \tag{7}$$

X and ϕ are the amplitude and phase angle which are obtained from the initial conditions of the system:

$$X = \sqrt{A^2 + B^2} = \sqrt{x_0^2 + \left(\frac{v_0}{\omega_n}\right)^2}$$

$$\phi = \tan^{-1}\left(\frac{v_0}{x_0\omega_n}\right)$$

A system with one DOF is not very accurate for most structures. It is therefore necessary to expand the system with more than one DOF. Determining the eigenfrequency for a system with more than one DOF is difficult and analytical solutions only exists for simple cases. The eigenfrequencies for a simply supported Bernoulli beam can be written as (Clough & Penzien, 2003, p. 380):

$$f_n = \frac{1}{2\pi}\left(\frac{n\pi}{L}\right)^2 \sqrt{\frac{EI}{\bar{m}L^4}}\,, n = 1,2,3,\ldots\text{k} \tag{8}$$

Where $\bar{m}$ is the weight per unit length, L is the total beam length and n is the eigenmode. The corresponding displacement, $u(x)$ can be defined as:

$$u(x) = \sin\left(\frac{n\pi x}{L}\right) \tag{9}$$

Eigenmodes and expressions for the eigenfrequencies for $n = 1,2$ are depicted in Figure 2.2

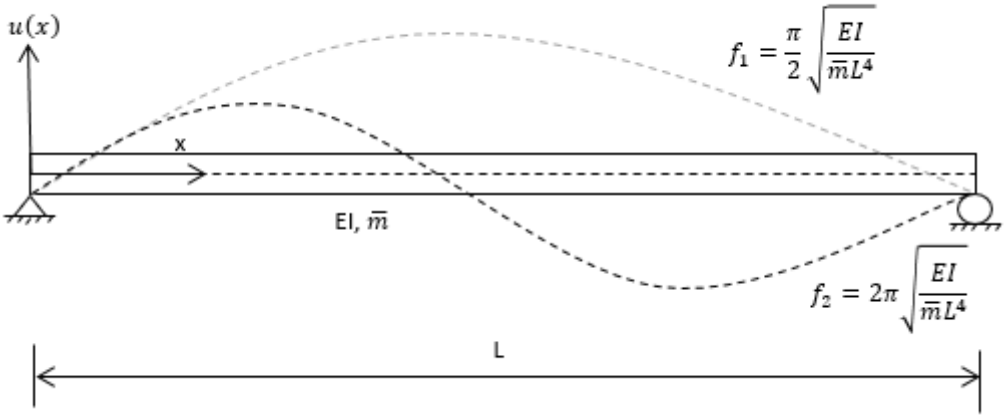

Figure 2.2- Analytical solutions for n=1,2 and corresponding natural frequencies

The equation of motion for an undamped free vibration MDOF system is given by the following matrix equation (Fu & He, 2001, p. 55-57):

$$\boldsymbol{M}\ddot{\boldsymbol{x}} + \boldsymbol{K}\boldsymbol{x} = \boldsymbol{0} \tag{10}$$

Where $\boldsymbol{M}$ the mass matrix, $\boldsymbol{K}$ is the stiffness matrix, $\boldsymbol{x}$ is the displacement vector and $\ddot{\boldsymbol{x}}$ is the acceleration vector. In order to compute the eigenfrequencies, the mass matrix and stiffness matrix needs to be computed. The non-trivial solution of equation (11) have the form:

$$\boldsymbol{x}(t) = \boldsymbol{\eta}\sin(\omega_n t) \tag{11}$$

Differentiate Equation (12) twice and insert in Equation (11) gives:

$$(\boldsymbol{K} - \omega_n^2\boldsymbol{M})\boldsymbol{\eta} = 0 \tag{12}$$

Equation (12) have a non-zero solution if $\boldsymbol{\eta}$ singular. The eigenvalue problem can thus be formulated as:

$$det(\boldsymbol{K} - \omega_n^2\boldsymbol{M}) = \boldsymbol{0} \tag{13}$$

By computing the determinant in equation (13), the eigenvalues and the corresponding eigenvectors can be obtained. The eigenvalues correspond to the square of the natural frequency, ω_i^2, and the eigenvector correspond to the mode shape, η_i. The roots of the equation ω_i^2 is the square of the natural frequencies $\omega_{n.i}$. The free vibration of the system depicted in Figure 2.2 can then be written as:

$$x_i(t) = \eta_i(t)\sin\left(\omega_{n,i}t\right), i = 1,2,\ldots,k \tag{14}$$

2.2 Undamped SDOF Harmonic Response Analysis

Harmonic response analysis is performed to determine the response of a structure under steady state conditions when subjected to sinusoidal (harmonic) loading for a range of frequencies. If the structure undergoes sinusoidal excitation in the form of an applied force: $f(t) = f_0 \sin(\omega t)$, the equation of motion for an undamped SDOF excitation is given by (Craig & Kurdila, 2006, p. 82-84):

$$\ddot{x} + \omega_n^2 x = f_0 \sin(\omega t) \tag{15}$$

The solution of equation (15) comprises of two parts: a homogenous solution and a particular solution. The homogenous solution of equation (15) is the same as the solution given by equation (7). Assume that the particular solution has the form:

$$x_p(t) = D \sin(\omega t) \tag{16}$$

Differentiating equation (16) and inserting in equation (15) gives the amplitude:

$$D\omega_n^2 - D\omega^2 = {f_0}/{m} \rightarrow D = \frac{{f_0}/{m}}{\omega_n^2 - \omega^2} = \frac{{f_0}/{k}}{1 - \frac{\omega^2}{\omega_n^2}} \tag{17}$$

Where $1 - \frac{\omega^2}{\omega_n^2} \neq 0$. Let $D_0 = \frac{f_0}{k}$, equation (17) can be expressed as:

$$\frac{D}{D_0} = \frac{1}{1 - \alpha^2} = \mathrm{H}(\alpha) \tag{18}$$

Where $\alpha = \frac{\omega}{\omega_n}$, $\mathrm{H}(\alpha)$ is the frequency-response function giving the magnitude and sign of the steady state solution as a function of frequency ratio, α. The steady state dynamic magnification factor, DMF_{ss} is given by the absolute value of frequency-response function (Craig & Kurdila, 2006, p.83):

$$DMF_{ss} = |\mathrm{H}(\alpha)| \tag{19}$$

Illustration of steady state DMF_{ss} for an undamped SDOF system is depicted in **Fel! Hittar inte referenskälla.**.

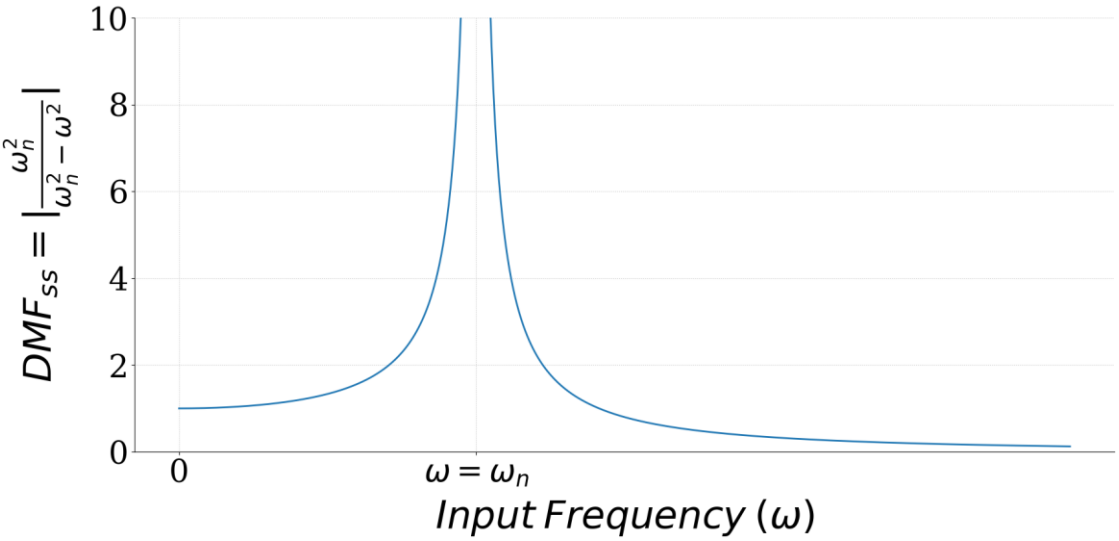

Figure 2.3 - Steady-state dynamic magnification factor for an undamped SDOF system subjected to sinusoidal excitation

The particular solution is given by inserting equation (18) in equation (17):

$$x_p(t) = \frac{f_0/k}{1-\alpha^2} \tag{20}$$

The total response is given by:

$$x_{tot}(t) = x_h(t) + x_p(t) = A\cos(\omega_n t) + B\sin(\omega_n t) + \frac{f_0/k}{1-\beta^2}\sin(\omega t) \tag{21}$$

Where A and B are integration constants to be determined by initial conditions.

2.3 RMS-value

The root mean square (RMS) value of a sinusoidal vibration with amplitude Δ_{max} is defined as the square of the peak amplitude of a sine wave, divide by two and take the square root (Siemens-simcenter, 2019) :

$$RMS = \sqrt{\frac{\Delta_{max}^2}{2}} = \frac{\Delta_{max}}{\sqrt{2}} \tag{22}$$

Equation (22) can be expanded to calculate RMS values of displacement, velocity and acceleration:

$$y_{RMS} = \frac{y_{max}}{\sqrt{2}}, v_{RMS} = \frac{v_{max}}{\sqrt{2}}, a_{RMS} = \frac{a_{max}}{\sqrt{2}} \tag{23}$$

Where subscript max represent peak amplitude value of a sine wave.

2.4 Modal superposition

2.4.1 Modal participation factor

The modal participation factor is used as a metric to quantify how much a vibration mode will be excited by a rigid body mode, $\boldsymbol{r}_j$. The modal participation factor, $\lambda_{i,j}$ of mode j triggered by a rigid body mode $\boldsymbol{r}_j$, is defined as (COMSOL, 2018):

$$\lambda_{ij} = \frac{\boldsymbol{\eta}_i^T \boldsymbol{M} \boldsymbol{r_j}}{\boldsymbol{\eta}_i^T \boldsymbol{M} \boldsymbol{\eta_i}} \tag{24}$$

For a translational rigid body mode $\boldsymbol{r}_j$, the displacement vector that has the values for displacement components in the direction of j and zero in all other components. $\boldsymbol{\eta}_i$ are the mode-shape vectors at mode i and $\boldsymbol{M}$ is the mass matrix. The denominator in equation (24) represent mass normalization, i.e.:

$$\widehat{M}_i = \boldsymbol{\eta}_i^T \boldsymbol{M} \boldsymbol{\eta_i} \tag{25}$$

Where $\widehat{M}_i$ is the modal mass. Due to the indeterminate size of $\boldsymbol{\eta}_i$, the term defined in equation (25) can be brought to one, i.e. $\widehat{M}_i = \boldsymbol{\eta}_i^T \boldsymbol{M} \boldsymbol{\eta}_i = 1$. If mass normalization of the modes is used, the modal participation factor can thus be expressed as:

$$\lambda_{ij} = \boldsymbol{\eta}_i^T \boldsymbol{M} \boldsymbol{r_j} \tag{26}$$

2.4.2 Effective Mass

Effective mass is defined as the inner product of the mode-shape vectors, given by equation (25). The effective modal mass is a quantity directly related to the modal participation factor (COMSOL – eigenfrequency analysis, 2018):

$$\widehat{m}_{eff,ij} = m_i \lambda_{ij}^2 \tag{27}$$

Where $\widehat{m}_{eff,ij}$ is the effective modal mass of mode i in the excitation rigid body mode direction j. The total mass of the structure is obtained by adding all effective modal masses in the direction j over all eigenmodes (COMSOL – eigenfrequency analysis, 2018):

$$\sum_{i=1}^{N_{eigenmodes}} \widehat{m}_{eff,ij} = m_{tot} \tag{28}$$

The physical interpretation of effective modal mass is that if an acceleration is in the direction of j, the effective modal mass can provide a method for judging how much of the total inertial force can be attributed to mode i. It can also provide a basis for an

estimation of how many modes that are needed for a response analysis. As a rule of thumb, the number of modes should at least be selected in such a way that the sum of all effective modal masses adds up to at least 90% of the actual mass of the system (Lopez. O.A, Cruz., M, 1996, p. 850).

2.5 Fatigue

In this section, a general background of fatigue will be provided.

2.5.1 Background

Material fatigue is the most common source behind structural failure. When a component or structure is subjected to a cyclic load that is above the material fatigue limit the material will fail. The process until a structure fails during cyclic loading can be divided into three factors (ASM International, 2008, p. 243):

- Sufficiently high values of maximum tensile stress
- Large enough fluctuations in the applied stress
- Sufficiently large number of cycles of the applied stress

In order to determine a material's endurance limit, i.e. the number of load cycles until failure, the load history has to be established. If the load history consists of constant amplitude stressing, the endurance limit can be evaluated directly. An illustration of constant amplitude stressing with notations is provided in Figure 2.4.

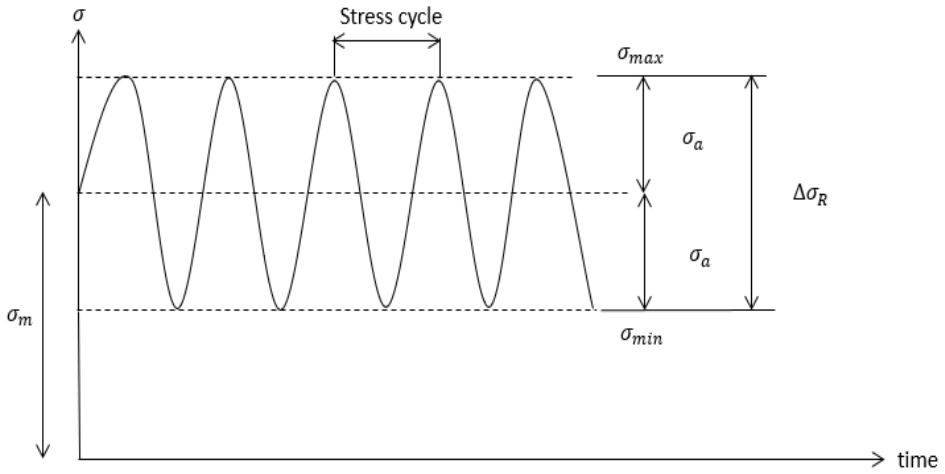

Figure 2.4 – Illustration of constant amplitude stress with notations

$\Delta\sigma_R$ is the stress range, σ_m is the mean stress and σ_a is the stress amplitude. Mathematical expressions for these definitions are provided below (Dowling, 2013 , p. 419):

$$\sigma_a = \frac{\Delta\sigma_R}{2} = \frac{\sigma_{max} - \sigma_{min}}{2} \tag{29}$$

$$\sigma_m = \frac{\sigma_{max} + \sigma_{min}}{2} \tag{30}$$

Other important parameters is the stress- and amplitude ratio. The stress ratio is defined as the ratio between maximum and minimum stress experienced during a stress cycle while the amplitude ratio is defined as the ratio of amplitude stress and mean stress:

$$R = \frac{\sigma_{max}}{\sigma_{min}} \tag{31}$$

$$A = \frac{\sigma_a}{\sigma_m} \tag{32}$$

By combining equation (30) with equation (31) an equation for the mean stress as a function of the stress amplitude ratio can be established:

$$\sigma_m = \frac{\sigma_{max}}{2}(1 + R) \tag{33}$$

It is worth noting that stresses can be positive or negative values. If stresses are negative it is referred to as compressive stress while positive values of stress is referred to as tensile stress. If the mean stress is zero, i.e $\sigma_m = 0$ then $R = -1$, this is known as a fully reversed cycle (Dowling, 2013, p. 420). If $\sigma_{min} = 0$, then $R = 0$, this is known as a zero-to-tension cycle (Dowling, 2013, p.420).

Fatigue is mainly classified into two types: High-cycle fatigue (HCF) and low-cycle fatigue (LCF). High-cycle fatigue occurs when a structure is failing due to small elastic strains under high number of loading cycles, typically in the order of $> 10^5$ cycles. Although the applied stress is sufficiently small to be considered elastic, a macroscopic plastic deformation can be observed at the crack tip. The yield stress is below the yield stress of the material (ASM International, 2008, p. 244). Low cycle fatigue on the other hand is the opposite of high cycle fatigue. LCF occurs due to large plastic strain and the macroscopic plastic deformation zone is larger than that in HCF. The stress level in LCF is in the elasto-plastic to plastic region. The stress level is higher than the endurance limit of the material and the amount of cycles until failure is usually in the range below 10^5 cycles (Agrawal, R., et.al, 2014, pp. 5-6).

2.5.2 Fatigue curve

A fatigue curve is a plot of nominal stress versus number of cycles until failure on a logarithmic scale. Nominal stress is defined as the stress calculated using general theories such as beam theory (IIW, 2008, p.9), meaning it does not include stress concentrations due to geometric discontinuities. Most design methods employ S-N curves as a tool to evaluate fatigue life. The shape curve or detail categories can differ between different design methods. The standard design code used as a reference code used to assess fatigue life is the EN 1993-1-9. In this code the fatigue life is evaluated by 14 different detail categories, defined as the nominal stress range after $N = 2 \times 10^6$ stress cycles which corresponds to the enduring limit, denoted as (1) in Figure 2.5.

Number of cycles level 2 in Figure 2.5 below represent the constant amplitude limit. For a structure only affected by a constant stress range, the predicted fatigue life can be obtained from the horizontal dotted design curves. The constant amplitude limit starts after $N = 5 \times 10^6$ cycles. However, if the stress range is varying the slope with $m = 5$ should be used. Number of cycles level 3 in the figure below represent the stress cut-off limit, $\Delta\sigma_L$ which correspond to $N = 10^8$ cycles, this is also known as the infinite lifetime region (Larsson 2009, p 30).

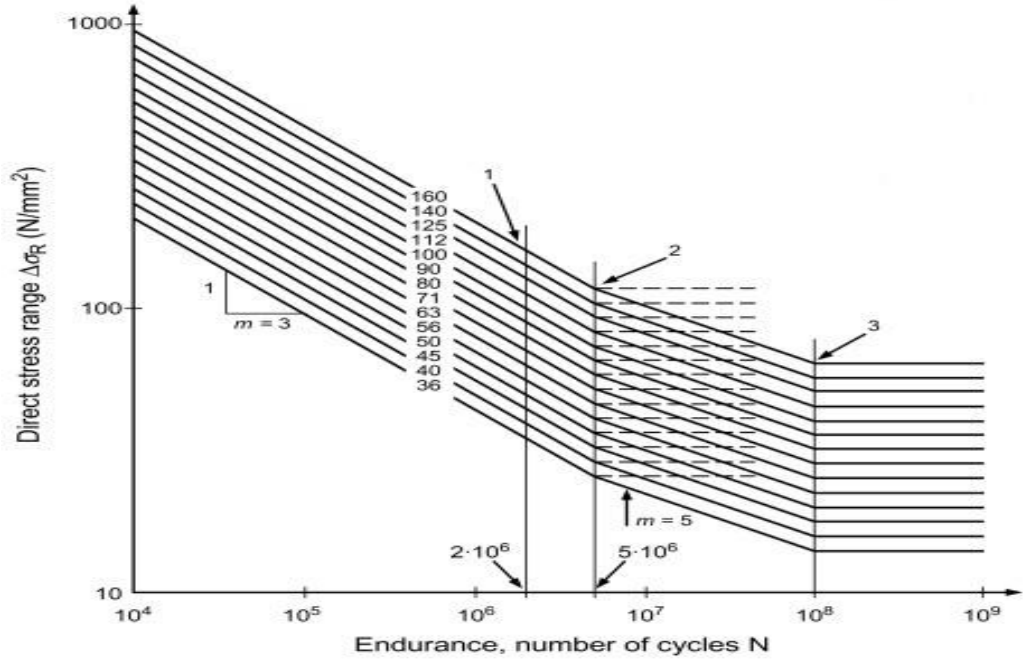

Figure 2.5- fatigue curves for nominal stress ranges

For constant amplitude nominal stresses, the fatigue limit of a structure can be expressed by the following relations (Eurocode 2004, 15):

$$\Delta\sigma_R^m \times N = \Delta\sigma_c^m \times 2 \times 10^6 \text{ with } m = 3 \text{ for } N \leq 5 \times 10^6 \text{ cycles} \quad (34)$$

where $\Delta\sigma_c$ is the detail category and $\Delta\sigma_R$ is the stress range. Equation (34) is valid for both constant and variable stress ranges. The constant amplitude fatigue limit can be calculated as:

$$\Delta\sigma_D = \left(\frac{2}{5}\right)^{1/3} \times \Delta\sigma_c = 0.737\Delta\sigma_c \quad (35)$$

For nominal stress ranges above and below the constant amplitude fatigue limit the fatigue strength is based on the extended curves in Figure 2.5:

$$\Delta\sigma_R^m \times N = \Delta\sigma_D^m \times 5 \times 10^6 \text{ with } m = 5 \text{ for } 5 \times 10^6 \leq N \leq 10^8 \quad (36)$$

The cut-off limit can be obtained by the following expression:

$$\Delta\sigma_L = \left(\frac{5}{100}\right)^{1/5} \times \Delta\sigma_D = 0.549 \times \Delta\sigma_D \quad (37)$$

2.5.2.1 Probability of failure

The probability density function curve for a standard normal variable z, which represents the bell-shaped curve of a normal distribution, can be used to identify probability of failure as illustrated in Figure 2.6 (Dowling 2013, pp. 902-904). A portion of the area under the density function curve gives the probability that z lies within the values that bound the area, i.e. there is approximately a 32% chance that a failure is expected to fall outside plus or minus one standard deviation. This can be used to identify limits corresponding to a probability of failure, such as $P = 0.001 = 0.1\%$, corresponding to one failure out of thousand tests.

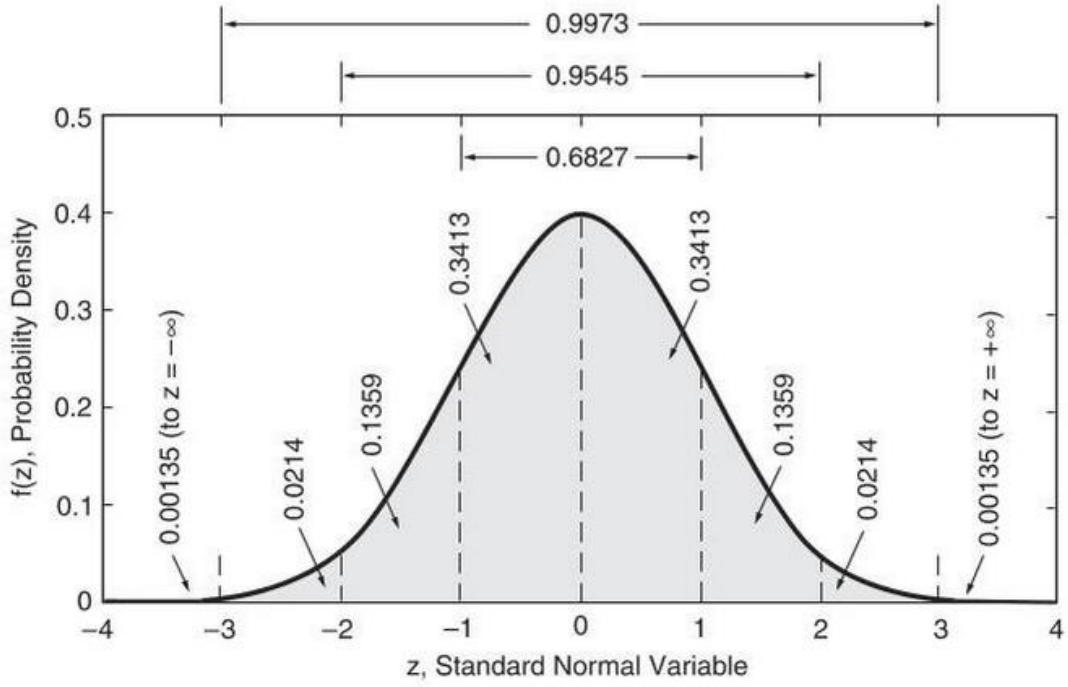

Figure 2.6 – Probability density function for the normal distribution from Dowling 2013. Portions of the area bounded by various numbers of standard deviations are shown (Dowling 2013, p.903).

2.5.3 Fatigue in welded structures

When assessing fatigue of a component, welded joints are crucial due to increased risk of crack initiation and low strength compared to the parent material. The welded joint will therefore limit the component strength against fatigue (IIW, 2008, p.41). Assessing fatigue strength of classified structures is often based on nominal stress ranges (IIW 2008, p.42).

Important regions are illustrated in Figure 2.7, where a butt weld is used as an example.

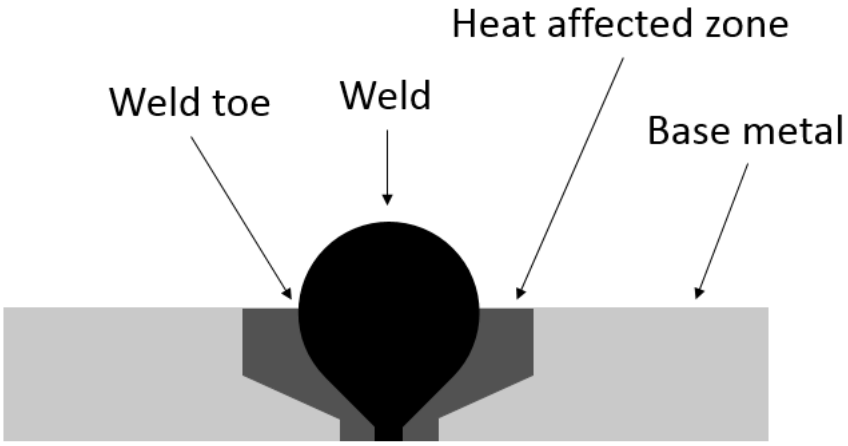

Figure 2.7 – A butt weld with important regions marked

Geometric discontinuities will increase the stress locally due to stress concentrations and in turn reduce the resistance to fatigue failure of a component. With the presence of a geometric discontinuity the stress will increase when approaching the weld toe as illustrated in Figure 2.8.

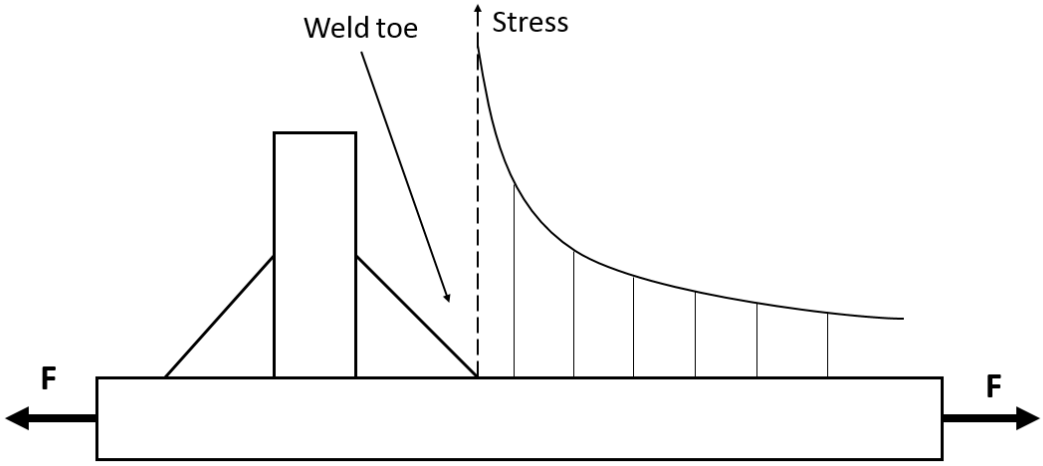

Figure 2.8 – Stress increase due to geometric discontinuity also referred to as notch stress

Weld joints are often subjected to high thermal strains during welding resulting in tensile residual stresses. Hence, when analysing components with welded joints the fatigue life, both magnitude and number of cycles will be lowered due to the fatigue sensitive weld. This is usually accounted for in S-N curves that are attained from welded test specimen (IIW 2008, p.77) and (SS-EN 2009, p.436-437).

2.6 The Finite Element Method

The finite element method (FEM) is a powerful tool used to approximate solutions of boundary value problems and is often used to determine mode shapes and natural frequencies of a structure in vibration. The basic idea with FEM is to discretize a structure into a finite number of elements and to find solutions that satisfy the partial differential equation within the boundary of the element. This is achieved by a set of polynomial functions that approximate the governing equations defined over each

element. In this way representations of stiffness and mass distribution can be obtained (Ottosen & Petersen, 1992, pp.1-2).

The sum of all elements in a computational domain is also known as a mesh. The mesh quality is important as a finer mesh enable the computer solution to approach the true solution. If u_h is the FE-approximation and $N_i(x)$ is the deflected shape functions and u is the displacement, the FE-approximation for a 1D element with 1 DOF for every node, u is approximated as (Möller. P, 2018, p. 9):

$$u \approx u_h = \sum_{i=1}^{n_{dof}} N_i(x) a_i \tag{38}$$

Where a_i is the unknown nodal variables and n_{dof} refer to the number of degress of freedom. Consequently, the FE-approximation for a 1D beam element with two translational DOF and an in-plane rotation DOF for every node is given by:

$$\begin{Bmatrix} u \\ v \\ \delta_z \end{Bmatrix} \approx \begin{Bmatrix} u_h \\ v_h \\ \delta_{zh} \end{Bmatrix} = \begin{Bmatrix} \sum_{i=1}^{n_{dof}} u_i N_i(x) \\ \sum_{i=1}^{n_{dof}} v_i N_i(x) \\ \sum_{i=1}^{n_{dof}} \delta_i N_i(x) \end{Bmatrix} \rightarrow \boldsymbol{u} \approx \boldsymbol{u_h} = \sum_{i=1}^{n_{dof}} \boldsymbol{a}_i \boldsymbol{N}_i(\boldsymbol{x}) \tag{39}$$

Where $\boldsymbol{u}_h$ is the FE-approximation, $\boldsymbol{a}_i = (u, v, \delta)$ is the unknown nodal quantities contained in node i. $\boldsymbol{x}$ is the position vector and $\boldsymbol{N}_i(\boldsymbol{x})$ is the deflected shape-functions in node i as a function of position. A 2-node beam element with 3 DOF at each node is depicted in Figure 2.9.

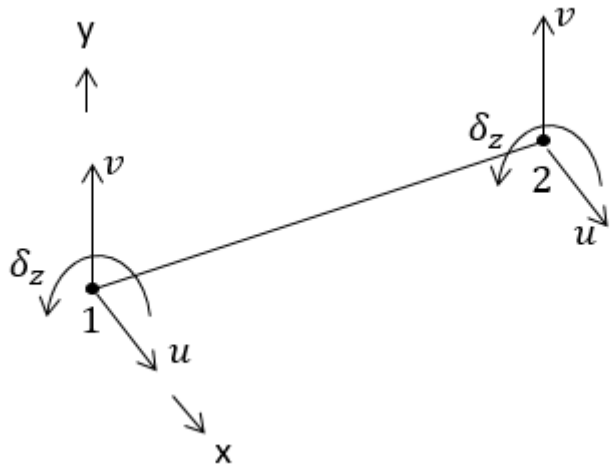

Figure 2.9 – Illustration of a 2-node beam element with 3 DOF

Where 1 and 2 is referred to 1:st and 2:nd node respectively. We can see that we need n_{dof} number of equations in order to solve for the unknown nodal variables.

2.6.1 Algorithm for solving vibration problems using FEM

The algorithm for obtaining solutions to structural problems using FEM is outlined below:

- Specify the computational domain. The domain can be constructed from a CAD model in ANSYS or in an external CAD- program.
- Define which element types that are to be used. In most commercial FE-software these are automatically defined in the program.
- Construct the mesh, i.e. divide the computational domain into small domains called elements. The sum of all elements in the computational domain is known as the mesh.
- Set up the simulation, define boundary conditions, prescribed loads and the number of modes that are appropriate in order to obtain a good solution.
- Run the simulation, the governing equations are solved within the boundary of each element.
- Post-processing. Extract relevant modes from the solution as well as other important parameters such as displacements, eigenfrequencies and stresses.
- Analyse and interpret the results

A commercial FE-code consists of three parts:

- Pre-processor – Generates the mesh and allows the user to set up boundary conditions, element types and potential loads on the system.
- Solver – Solves the system of discretized governing equations in the form of algebraic equations.
- Post-processor – Gives the user the ability to interpret the results from the solution.

3 Methodology

In this chapter the computational models used to compare the methods are presented in order of increasing complexity. This is followed by a description of each code of practice and the chapter ends with data extraction from ANSYS Workbench R2.

3.1 Computational models

FE-analysis on all computational models are conducted using ANSYS Workbench 2019 R2. All computational models are modelled as thin walled structures and quad/Tri solid-shell elements. Computational model 1 include MASS21, SOLSH190, conta175 and TARGE170 elements. Elements used in computational model 2 include the same elements as in computational model 1 with the inclusion of COMBIN14 elements for springs. Computational model 3 include same elements as in computational model 2. All elements used in the simulations are discussed more thorough in Appendix D. Modal analysis is performed to obtain eigenfrequencies, eigenmodes and stresses for all three computational models. Harmonic response analysis is performed on the third computational model to obtain frequency response spectrum when subjected to an applied uniform acceleration amplitude.

Modal analysis for all three models is divided into three simulations:

1. Investigate the impact on allowable vibration velocity for varying added concentrated mass considering one eigenmode.

2. Investigate the impact on allowable vibration velocity for varying eigenmodes without added concentrated mass. Eigenmodes are selected based on:
    i. For computational model 1 eigenmodes are selected based on eigenmodes with pure bending.
    ii. For computational model 2 and 3 eigenmodes are selected based on eigenmodes with highest modal participation factor.

3. Combination of 1. and 2.

3.1.1 Material properties

For all three models an isotropic linear elastic low alloy steel material is used. The pipes are simulated as filled with liquid water. Material properties are summarized in Table 3.1.

Table 3.1 - Material properties for low alloy steel at room temperature (20°C) obtained from ANSYS Workbench 2019 R2

Density pipe - ρ_{pipe} $\left[\frac{\text{kg}}{\text{m}^3}\right]$	7850
Density medium - ρ_{med} $\left[\frac{\text{kg}}{\text{m}^3}\right]$	1000
Elasticity modulus - E [GPa]	200
Poisson's ratio - ν [-]	0,3
Bulk modulus - K [GPa]	167
Shear modulus - μ [GPa]	76,9
Coefficient of thermal expansion - β $[K^{-1}]$	$1{,}2 \times 10^{-5}$

The weight of water inside the pipe was accounted for by increasing the density of the pipe material accordingly:

$$\rho_{tot} = \frac{m_{med}}{V_{pipe}} + \rho_{pipe} \tag{40}$$

3.1.2 Computational model 1

Computational model 1 represents a typical straight piping section with fixed ends and a concentrated body mass, M, in the middle, which can be represented by a pump or valve. The dimensions of the pipe are summarized in Table 3.2.

Table 3.2 – Dimensions for computational model 1

Outer diameter D_o [mm]	**Wall thickness** t [mm]	**Length** L [mm]	**Concentrated mass** M [kg]
114,3	2,9	3300	400/40/0

The chosen boundary conditions for computational model 1 are fixed at both ends to avoid rigid body motion. Concentrated mass is located at the centre of the pipe. The boundary conditions are illustrated in Figure 3.1.

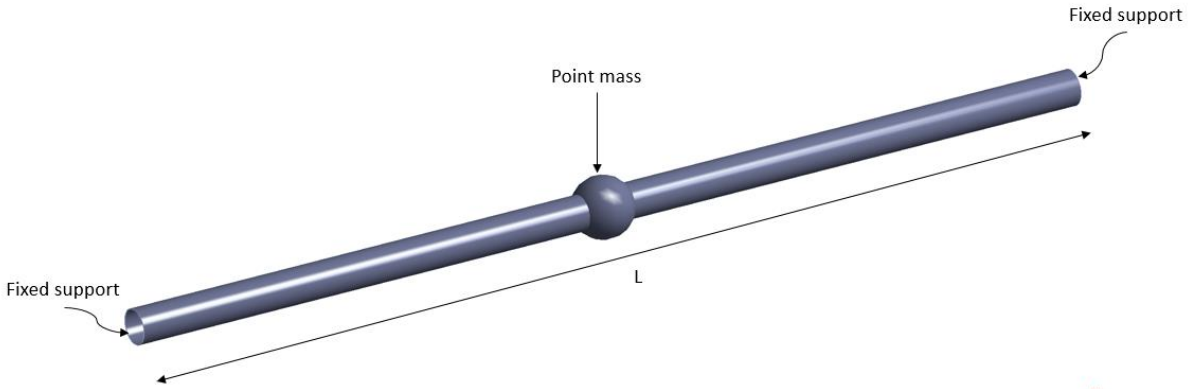

Figure 3.1 - Illustration of the geometry for computational model 1 with prescribed boundary conditions

3.1.3 Computational model 2

Computational model 2 represents a typical pipe configuration that can be mounted on a larger pipe for easier access. Computational model 2 consists of straight sections with a series of 90° elbow bends and fixed support at both ends to avoid rigid body motion. The model also includes a spring support and concentrated varying mass where the model is illustrated in Figure 3.2. The dimensions of the pipe are summarized in Table 3.3.

Table 3.3 - Dimensions for computational model 2

Outer diameter D_o [mm]	**Wall thickness** t [mm]	**Length** $L_1/L_2/L_3$ [mm]	**Radius** R	**Concentrated mass** M [kg]	**Spring stiffness** $k_x/k_y/k_z$ $[kN/mm]$
60,3	3,2	300/450/300	100	10/1/0	200/0,4/0,4

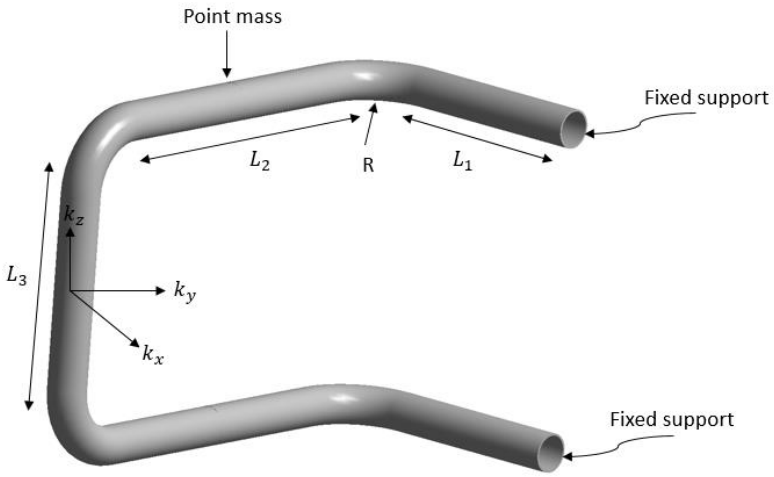

Figure 3.2 - Illustration of the geometry for computational model 2 with prescribed boundary conditions

3.1.4 Computational model 3

Computational model 3 represents a more complete piping system compared to computational model 1 and 2. Computational model 3 is considered the most complex regarding dimensions and number of suspensions included. Computational model 3

consists of a straight pipe section followed by a series of elbow bends and fixed at both pipe ends to avoid rigid body motion. The model includes spring supports, varying concentrated mass and the model is illustrated in Figure 3.3. Pipe dimensions are summarized in Table 3.4. The structure is excited by a prescribed uniform acceleration amplitude.

Table 3.4 – Dimensions for computational model 3

Outer diameter D_o [mm]	**Wall thickness** t [mm]	**Length** $L_1/L_2/L_3$ $/L_4/L_5$ $/L_6$ $/L_7$ [mm]	**Radius** $R_1/R_2/R_3$ $/R_4$ $/R_5$ $[mm]$	**Concentrated mass** M [kg]	**Spring stiffness** k_x $/k_y/k_z/$ $k_{pre-comp,1z}/$ $k_{pre-comp,2z}$ [kN/mm]	**Spring pre-compression force** $F_{pre-comp,1z}/$ $F_{pre-comp,2z}$ [kN]
273	6,3	32415 /2310 /2645 /5150 /1848 /3041 /692	383 /383 /383 /383 /383	200/20/0	90000 /90000 /90000 /65,4 /32,7	5,94/8,77

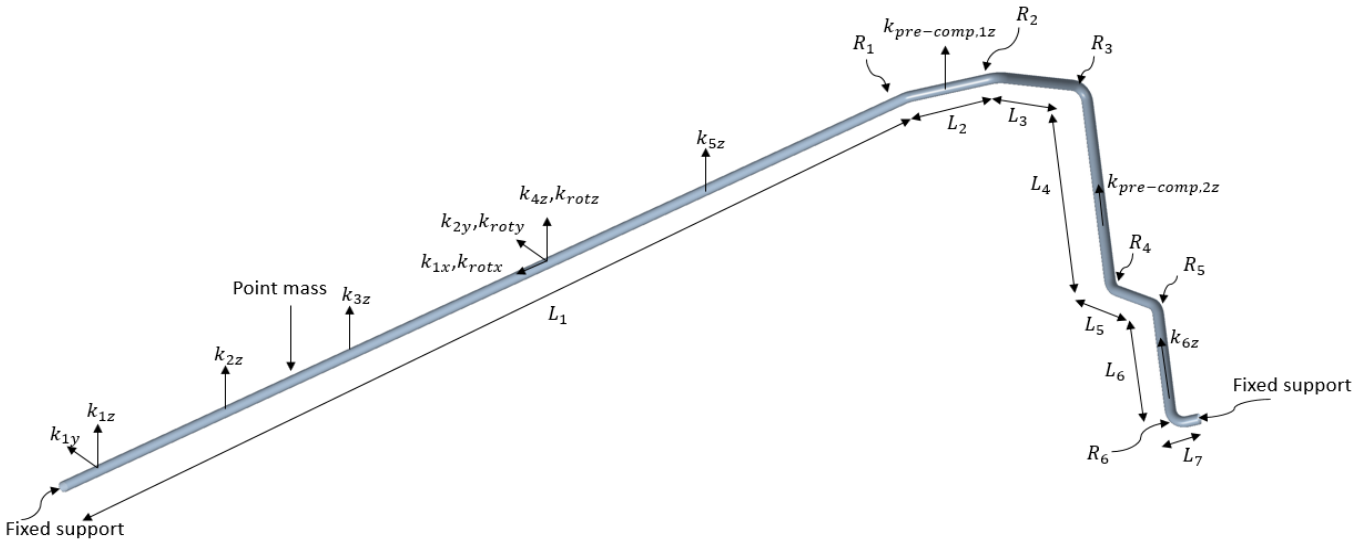

Figure 3.3 – Illustration of the geometry for computational model 3 with prescribed boundary conditions

3.2 Industrial methods

Important sections regarding fatigue assessment during vibration are summarized in the following sections for each code to give an overview of how the methods is used to determine allowable vibration velocity levels.

3.2.1 ASME OM-2015

ASME OM-2015 presents two types of methods to assess allowable vibration velocity levels of piping systems during plant operation. A simplified method for qualifying piping systems and a more rigorous verification method for steady-state and transient vibration. In regard to determine an allowable vibration velocity, two methods in ASME OM are applicable, described in 3.2.1.4.

Fatigue assessment in ASME OM utilize coefficients and fatigue data defined in ASME BPVC which is a comprehensive method for design and analysis of boilers and pressure vessels.

3.2.1.1 Classification of components

ASME BPVC divide components in a nuclear power system into three classes based on level of importance associated with safe operations of the nuclear power plant. Each classification include rules assuring structural integrity and quality proportional to the importance assigned, where class 1 implies highest importance and 3 are assigned with lowest importance.

3.2.1.2 Design fatigue curves

Assessment of fatigue failure due to pipe vibrations presented in ASME OM-2015 is based on fatigue curves in ASME BPVC 2017 section 3 appendix 1. From an allowable alternating stress for a specified material the allowable vibration velocity is calculated. The alternating stress used to calculate ASME allowable vibration velocities is obtained from carbon steel fatigue data (ASME BPVC, 2017, section III, Table I-9.1):

$$S_{el} = 86\ MPa \tag{41}$$

$S_{el} = 0.8S_a$, where S_a is alternating stress at 10^6 cycles (endurance limit), obtained from ASME BPV, section 3, Table I-9.1, or S_a at 10^{11} cycles (endurance limit) from ASME BPV, section 3, Table I-9.2 An extension of fatigue strength for all methods is presented in Table 7.1 Appendix A.

Fatigue curves in ASME BPVC 2017 section 3 appendix 1 for carbon steel and austenitic steel are based on uniaxial strain cycling data where imposed strain amplitude (half range) is multiplied by the elastic modulus converting the values to stress (ASME BPVC 2017 section 3, mandatory appendix 3, p.39). ASME BPVC 2017 present a best fit curve which was obtained with the least squared method from logarithmic stress values. ASME BPVC 2017 have also adjusted the curves where necessary to include the maximum effect of mean stress. From ASME BPVC 2017 the design fatigue strength values can be obtained for carbon steel from the best fit curve by applying a factor of 2 on stress or a factor of 20 on cycles, whichever is the more conservative at each point. For austenitic steel ASME proposes a factor of 2 on stress or a factor of 12 on cycles, whichever is the more conservative at each point (ASME BPVC 2017 section 3, mandatory appendix 3, p.39).

3.2.1.3 Stress indices

ASME OM-2015 is used to calculate allowable vibration velocity levels from design fatigue curves based on nominal alternating stress. In order to account for geometrical discontinuities and welds, stress indices are utilized.

3.2.1.3.1 Weld joints

The stress indices for weld joints are determined dependent on the component classification which are defined for each methods.

3.2.1.3.2 Class 1 components - NB

ASME BPVC 2015 subsection NB define the stress index for a mechanical load as (ASME BPVC 2015, section III, subsection NB, p.126):

$$C_2, K_2 = \frac{\sigma}{S} \quad (42)$$

where
S = nominal stress MPa
σ = elastic stress MPa

For C or K, σ represents maximum stress intensity due to a load L.

The stress indices given in Figure 7.11 in appendix A are applicable to girth butt welds connecting adjacent products for which the wall thickness is between $0.875t$ and $1.1t$ for an axial distance of $\sqrt{D_o t}$ from the welding ends and $D_o/t \leq 100$. For as-welded girth butt welds joining items with nominal wall thicknesses $t < 6.0\ mm$, the C_2 index shall be taken as (ASME BPVC 2015, section III, subsection NB, p.131):

$$C_2 = 1 + \frac{2.4}{t}, \text{but not } > 2.1 \quad (43)$$

for $t > 6\ mm$, $C_2 = 1$

Stress index for ASME class 1 as-welded girth butt weld is summarized for all computational models in Table 3.5. All welded results illustrating ASME are calculated with these indices.

Table 3.5 – Summary of ASME class 1 stress index of as-welded girth butt weld for the three computational models.

	$t\ [mm]$	C_2	K_2	C_2K_2
Computational model 1	2.9	1.83	1.8	3.3
Computational model 2	3.2	1.75	1.8	3.15
Computational model 3	6.3	1.38	1.8	2.48

3.2.1.3.3 Class 2 & 3 components - NC & ND

ASME BPVC 2015 subsections NC & ND define the stress intensification factor based on fatigue bend testing of mild carbon steel fittings as (ASME BPVC 2015, section III, subsection NC, p.152):

$$iS = 1700N^{-0.2} \quad (44)$$

Where:
i is the stress intensity factor which is defined as the ratio of the bending moment producing fatigue in a given number of cycles in a straight pipe with a girth butt weld to failure with the same number of cycles in the fitting or joint under consideration.
N = number of cycles to failure
S = amplitude of the applied bending stress at fatigue failure, MPa

For piping configurations or joints not defined in ASME BPVC 2015 subsections NC & ND, stress intensification factors should be established by experimental or analytical means. Analytical determination of stress intensification factors may be based on the empirical relationship (ASME BPVC 2015, section III, subsection NC, p.160):

$$i = C_2 K_2/2, \text{ but not} < 1 \tag{45}$$

where C_2 and K_2 are stress indices for Class 1 piping configurations or joints.

ASME class 2 and 3 components define the stress intensity factor, i, equal to 1 for girth butt welds, applicable when $D_o/t \leq 100$ (ASME BPVC, section III, subsection NC, p.156).

3.2.1.4 Methods of evaluating allowable vibration velocity levels

Standard ASME OM-2015 evaluates pipe vibrations by calculating an allowable vibration velocity. Allowable vibration velocity is compared with measured maximum vibration velocity in order assess whether the piping system fulfil the criteria for qualification. In ASME OM-2015, a screening value of velocity can be calculated to verify if this velocity fulfils the following equality (ASME-OM 2015, p. 118):

$$v_{max} \leq v_{allow} \tag{46}$$

If this criterion is not fulfilled, a more advanced and less conservative method should be employed to determine allowed peak velocity. This method uses alternating stress and modal analysis using FE-analysis to obtain maximum allowable vibration velocities.

3.2.1.4.1 Handbook evaluation for determine allowable peak velocity

This method gives a screening value of allowable vibration velocity. Allowed vibration velocity according to ASME OM-2015 is given by (ASME-OM 2015, p. 128):

$$v_{allow} = \frac{C_1 C_4 \beta(S_{el})}{C_3 C_5 \alpha C_2 K_2} \tag{47}$$

Where:

v_{allow} is the allowable peak velocity in $\left(\frac{mm}{s}\right)$

C_1 is a correction factor that compensate the effects of concentrated weights. If concentrated weight is less than 17 times the pipe span weight a conservative value of 0.15 can be used for screening purposes.

$C_2 K_2$ are stress indices, found in ASME BPVC 2015, Section III, p. 127 Table NB- 3681(a).

C_3 is a correction factor accounting for insulation and pipe content and is defined as:

$$C_3 = \left(1 + \frac{W_f}{W} + \frac{W_{INS}}{W}\right)^{1/2} \tag{48}$$

W_f is the fluid weight per unit length, W_{INS} is insulation weight per unit length and W is the pipe weight per unit length.
C_4 is a correction factor for different piping configurations:
$= 1$ for a straight span fixed at both ends
$= 1.33$ for a cantilever and simply supported pipe span
$= 0.74$ for a z-bend with equal leg
$= 0.83$ for a U-bend with equal leg
C_5 is a correction factor to be used when the measured frequency differs from the first eigenfrequency of the piping span.

If $\frac{f_n}{f_{measured}} < 1$, $C_5 = 1$

If $\frac{f_n}{f_{measured}} > 2$, equation (47) is not valid

$S_{el} = 0.8S_a$, where S_a is alternating stress at 10^6 cycles, taking from ASME BPV, section 3, Table I-9.1, or S_a at 10^{11} cycles from ASME BPV, section 3, Table I-9.2
β is a conversion factor of 13.4 to obtain v_{allow} in $\left(\frac{mm}{s}\right)$ when S_a is expressed in MPa
α is the allowable stress reduction factor:
$= 1.3$ for materials (carbon steel) in ASME BPV, section 3, Table I-9.1
= 0.8 for materials (stainless steel) in ASME BPV, section 3, Table I-9.2

Safe levels of vibration can be chosen by taking conservative values of the correction factors defined above. The screening velocity criterion holds for any pipe configuration. For conservative screening purposes, values of the different correction factors are presented in Table 3.6:

Table 3.6 - Conservative values of correction factors for screening purposes.

C_1	C_2K_2	C_3	C_4	C_5	$\frac{0.8S_a}{\alpha}$ $[MPa]$	β
0.15	≤ 4	1.5	0.7	1	53	13.4

From Table 3.6, a conservative screening value of allowed peak velocity can now be obtained by using equation (99):

$$v_{allow} = \frac{0.15 \times 0.7 \times 13.4 \times 53}{1.5 \times 4 \times 1} = 12.4 \frac{mm}{s} \quad (49)$$

It should be noted that this screening value is very conservative and thus should be seen as a reference value. When changing material and geometrical properties, a less conservative value of allowed velocity is obtained.

3.2.1.4.2 Evaluation of allowable peak velocity using FEM

If $v_{max} \geq v_{allow}$ more accurate values of the correction factors need to be determined so that an acceptable velocity criterion can be established for the piping configuration. A more advanced method involving FE-analysis can be employed to calculate a less conservative and more accurate value of allowable peak vibration velocity. This method

involves calculating allowable alternating stress according to equation (50). Allowable peak vibration velocity is then to be determined from stress analysis given by modal synthesis. From modal synthesis, bending stress and modal displacements can be obtained for each eigenmode. And the relation between modal stress and displacement holds and from that an allowable peak velocity can then be determined.

3.2.1.4.2.1 Calculation of allowable maximum velocity

For steady state vibrations using maximum alternating stress intensity, s_{alt}, is given by the following relation (ASME-OM, 2015, p. 113-114):

$$s_{alt} = \frac{C_2 K_2}{Z} M_{b,max} \leq \frac{S_{el}}{\alpha} \tag{50}$$

Where Z is the section modulus of the pipe, $M_{b,max}$ is the maximum zero-to-peak bending moment due to vibration, or in combination with other loads. C_2K_2, α and S_{el} is defined in section 3.2.1.4.1. Maximum modal bending stress can be written as:

$$\sigma_{b,max,j} = \frac{C_2 K_2}{Z} M_{b,max,j} \tag{51}$$

Where j denotes the eigenmode. The fact that modal stress is proportional to modal displacement, the modal velocity for eigenmode j can be defined as:

$$v_{modal,j} = 2\pi f_j \delta_j \tag{52}$$

Where f_j is the eigenfrequency at eigenmode j and δ_j is the displacement at eigenmode j. From Equations (49)-(51), an expression for maximum allowable RMS velocity can be obtained for j:th eigenmode:

$$v_{RMS,allow,j} = \frac{v_{modal,j} S_{el}}{\sqrt{2}\alpha \sigma_{b,max.j}} \tag{53}$$

Where j denotes j:th eigenmode. When computing vibrations, it is important to establish a computational model with high geometric certainty in order to accurately predict eigenfrequencies and eigenmodes. Measurements of the piping system should be carried out in order to determine the real eigenfrequencies and eigenmodes of the system. The computational model should thereafter be calibrated to correspond with measurements. Calibration of the computational model could involve changing stiffness and mass. This could be done by changing the diameter, length, spring stiffness constants or concentrated mass of the piping system.

3.2.2 SS-EN-13445-3

Standard SS-EN-13445-3 does not include explicit methods for calculating an allowable vibration velocity. However, vibration velocity can be calculated using alternating stress amplitude from design fatigue curves and modal analysis. Utilizing the linear relation between modal stress and modal deflection, modal deflection is scaled corresponding to modal stress matching the stress amplitude from fatigue curves. With modal deflection corresponding to fatigue failure, an allowable vibration velocity can be calculated from equation (52).

SS-EN 13445-3 present a detailed assessment of fatigue life of pressure vessels and their components that are subjected to repeated stress fluctuations. Fatigue in welds will behave differently from unwelded material and therefore SS-EN 13445-3 divide fatigue assessment into welded and unwelded components.

3.2.2.1 Design fatigue curves for unwelded components

Design fatigue curves for unwelded components can be applied to certain tensile strength of steel. Design fatigue curves for unwelded components in SS-EN-13445 have been derived from fatigue test specimens obtained during alternating (mean load=0) load control, or from applied strains exceeding the yield limit (SS-EN-13445, 2009, part 3, chapter 18, p. 498). Compared with the mean curve fitted to the original data, the curves incorporate safety factors of 10 on fatigue life and 1,5 on stress range (SS-EN-13445, 2009, part 3, chapter 18, p. 498):

The alternating stress used to calculate unwelded EN allowable vibration velocity is obtained from fatigue data (SS-EN-13445, 2009, part 3, chapter 18, Table 18-10):

$$S_a = 152.25\ MPa \tag{54}$$

where S_a is half the stress range at 2×10^6 cycles (endurance limit), obtained from SS-EN-13445 Table 18-10 for a tensile strength of 450 MPa.

3.2.2.2 Design fatigue curves for welded components

Design fatigue curves for welded components can be applied to particular construction details. The curves are identified by the fatigue strength value $\Delta\sigma_R$ at fatigue life $N = 2 \times 10^6$ cycles. Alternating stress used to calculate welded allowable vibration velocity is obtained from fatigue data (SS-EN-13445, 2009, part 3, chapter 18, Table 18-7):

$$S_a = 23\ MPa \tag{55}$$

where S_a is half the stress range at 5×10^6 cycles (endurance limit), obtained from SS-EN-13445 Table 18-10 for a tensile strength of 450 MPa.

SS-EN-13445 gives design fatigue curves from fatigue test data obtained from appropriate laboratory specimens, tested under load control or from applied strains exceeding the yield limit during strain control (SS-EN-13445, 2009, part 3, chapter 18, p.491). Continuity from low to high cycle regime is achieved by expressing the low cycle fatigue data in terms of pseudo-elastic stress range, i.e. strain range multiplied by elastic modulus. The failure criteria on which these curves are based on is break-through of the weld or parent metal. This data is compatible with results obtained from pressure cycling tests on actual vessels. Fatigue design curves are approximately three standard deviations of log N below the mean curve, fitted to the original test data by regression analysis. Thus, they represent a probability of failure of approximately 0.14% (SS-EN-13445, part 3, p.491).

3.2.2.2.1 Evaluation of allowable peak velocity using FEM

An allowable peak velocity is calculated in a similar manner as ASME. Deformations and stress intensities are scaled by a factor that matches half stress range from design fatigue curves. The scaling of deformations and stress intensities is valid since relationship between them is linear in modal analysis.

3.2.3 VDI 3842/KTA 3211

The guideline VDI 3842 merely provides an overview on evaluating fatigue and strength for piping systems, where relevant methods applicable to industries are referenced for further details. The prime objective of the guideline is to facilitate working with the special methods summarized in Table 3.7.

Table 3.7 - Methods related to pipes in different power plants.

Code	Area of application
FDBR guideline	Power station pipes
KTA 3201, KTA 3211	Pipes in nuclear power stations
ASME/ANSI B31.1	Power piping
ASME/ANSI B31.3	Chemical plant and petroleum refinery piping
DIN EN 13 480	Metallic industrial piping

From methods listed in Table 3.7, KTA 3211 is selected for finding methods to calculate allowable vibration velocity levels due to its application in nuclear power stations. The following subsections are based on this code.

3.2.3.1 Design fatigue curves

Similar to ASME BPV Code, KTA 3211 include design fatigue curves for unwelded components where effects of welded joints are included by utilizing stress indices.
The methods do not specify how the fatigue curves included in KTA 3211.2:2013-11 are derived and they are used as a reference included in Appendix B.

Alternating stress used to calculate unwelded KTA allowable vibration velocity is obtained from fatigue data (KTA3211, 2013, part 2, Table 7.8-3):

$$S_a = 86.2\ MPa \tag{56}$$

where S_a is half the stress range at 1×10^6 cycles (endurance limit).

3.2.3.2 Stress indices

Fatigue analysis described in KTA 3211.2 follows the same procedure as ASME OM-2015 where allowable RMS vibration velocity levels are calculated from design fatigue curves based on nominal alternating stress. Effects of geometrical discontinuities and weld joints are included with stress indices, analogous to ASME OM-2015.

3.2.3.2.1 Weld joints

Including weld joints in a structure is crucial for the assessment of fatigue failure as described in section 3.2.1.3.1. Analogous to ASME OM-2015, KTA 3211 include stress indices to account for the effects of weld joints.

Stress indices given in Figure 7.16 appendix A are applicable to butt welds for items with same nominal thickness.

3.2.3.2.2 Screening values for allowable vibration velocities

According to VDI 3842 an initial assessment of pipe stresses can be carried out with the use of vibration velocity and the proportional relation between stress and vibration velocity (VDI 3842:2004-6, p. 63). Based on this proportionality investigations have been done in the past to develop procedures for assessing pipe vibrations (VDI 3842:2004-6, p. 63). An initial screening value for allowable RMS vibration velocity could be obtained by reading design or danger lines in Figure 3.4. These values are based on experience in the petro-chemical industry over a period of more than 25 years and are applicable for pipes which have geometries and support spacing common in the petrochemical industry.

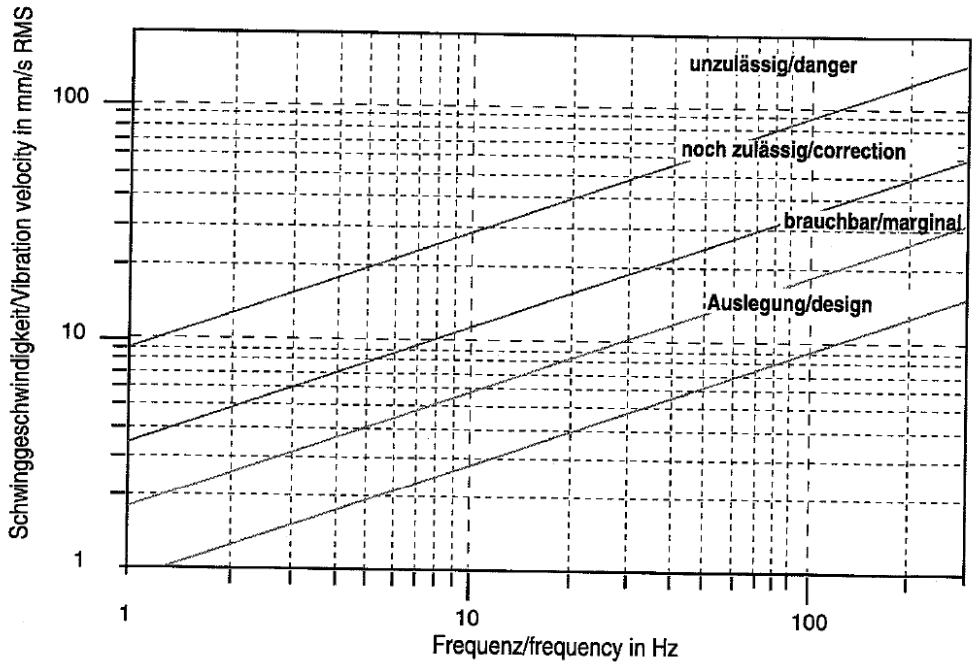

Figure 3.4 – Orientation values for permissible pipe vibrations from VDI 3842:2004-6, Fig 7.4

3.2.3.2.3 Handbook evaluation for determine allowable peak velocity

An extension to cover all types of piping for the method of assessing stress from vibration velocity is the analytic solution presented below (VDI 3842:2004-6, p. 64):

$$\sigma_{\max} = f_M f_i f_\phi v_{max} r_a \sqrt{\frac{E\mu}{I}} \tag{57}$$

Where:

f_ϕ is the mode index dependent on the mode characteristic $f_\phi = \phi''_{n,max}/\phi_{n,max}$ with the curvature ϕ''_k of the n^{th} mode, found in VDI table 7.1 (VDI 3842:2004-6, p. 63).
f_i is the stress increase factor, found in VDI table 7.4 (VDI 3842:2004-6, p. 63).
f_M is the correction factor for concentrated masses, found in VDI figure 7.5 (VDI 3842:2004-6, p. 63).
v_{max} is the maximum vibration velocity.
μ is the mass loading.
E is the modulus of elasticity.
I is the moment of inertia.
r_a is the external pipe radius.

Equation (57) is used to calculate the allowable vibration velocity by substituting the maximum stress with alternating stress amplitude, S_a.

3.2.4 International institute of welding

Allowable vibration velocity levels for welded components can also be calculated with alternating stress amplitude from design fatigue curve containing fatigue classes. A fatigue class is the fatigue strength of components expressed in units of MPa at $N = 2 \times 10^6$ cycles. Fatigue classes for specific welds can be obtained from IIW, Tab. {3.2}-1. For instance, the transverse butt weld illustrated in Figure 3.5 has a fatigue class of 71 MPa (IIW, 2009, Tab. {3.2}-1, p.52).

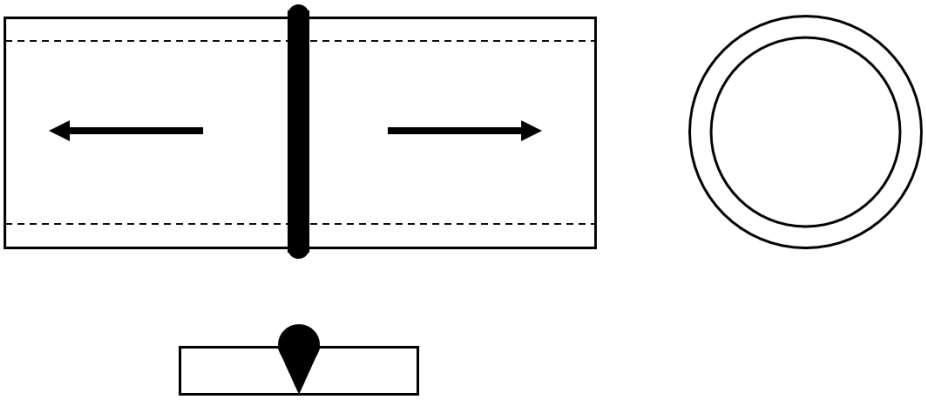

Figure 3.5 - Transverse butt weld in circular hollow section, welded from one side, full penetration

3.2.4.1 Design fatigue curves

According to IIW fatigue assessment of classified components and weld joints is based on nominal stress range, where in most cases components are assessed on the basis of maximum principal stress range in the section critical to fatigue cracking. Design fatigue curves for normal stress ranges and weld classifications are illustrated in Figure 7.17 and Figure 7.18 in appendix A. Fatigue strength data from IIW represent a survival probability of at least 95% (IIW 2008, p.41).

The alternating stress used to calculate welded IIW allowable vibration velocity is obtained from fatigue data (IIW, 2008, Figure(3.2)-2):

$$S_a = 20.5\ MPa \tag{58}$$

where S_a is half the stress range at 1×10^7 cycles (endurance limit), obtained for a fatigue class of 71 from IIW Tab. {3.2}-1.

3.2.5 Allowable vibration velocity from fatigue data

Allowable vibration velocity for methods without an explicit equation are calculated by scaling the largest displacement from ANSYS with a ratio corresponding to the alternating stress from fatigue curve and maximum stress in ANSYS:

$$\delta_{allow} = \delta_{ANSYS} \frac{S_a}{\sigma_{max,ANSYS}} \tag{59}$$

The allowable vibration velocity can be determined from equation (52) and (53).

3.3 Data extraction from modal analysis

Eigenmodes and corresponding eigenfrequencies were calculated in ANSYS with modal analysis. The largest total deformation and maximum stress intensity for the models were extracted for each eigenmode. This is based on the assumption that the largest deformation will correspond to the highest stress intensity. Due to the high number of eigenmodes for each computational model and the fact that a manual inspection is required for each mode, a selection of the most important eigenmodes was necessary. The number of eigenmodes included in the solution were selected such that the accumulation of effective mass at least exceeds 90 % of the total mass of the system. From this set of eigenmodes an additional selection based on eigenmodes with highest modal participation factor were performed for a given frequency range of 0-100 Hz.

3.4 Data extraction from harmonic analysis

Eigenfrequencies and eigenmodes are extracted from harmonic response analysis for computational model 3 when subjected to an excitation load in the form of a prescribed acceleration amplitude. Largest deformation and stress intensity are extracted from the forcing frequency range to calculate allowable RMS vibration velocities. Frequencies within 0.5 Hz of each other were selected based on the highest ratio of stress intensity and deformation since this will yield lowest allowable vibration velocity.

4 Results

In this chapter results for all computational models are presented in the form of allowable vibration velocity levels as a function of frequency. Results are presented in numbering order, beginning with computational model 1 and ends with computational model 3. Vibration mode shapes are illustrated as contour plots extracted from FE-simulations. Allowable vibration velocity levels from VDI graph (Figure 3.4) are included as a reference value, included in all result diagrams.

4.1 Computational model 1

Results for model 1 are divided into four parts:

i. Illustration of extracted bending mode shapes used to determine allowable RMS vibration velocities.
ii. Study of concentrated mass and eigenmodes for an unwelded pipe.
iii. Study of concentrated mass and eigenmodes for a welded pipe.
iv. Combination of concentrated mass for varying eigenmodes.

4.1.1 Vibration mode shapes

The eigenmodes used to determine allowable RMS vibration velocity diagrams for computational model 1 are illustrated in Figure 4.1. Mode shapes coloured with red represent maximum deformation and blue represent minimum deformation. Participation factors and eigenfrequencies for the eigenmodes are summarized in Table 4.1for the case of a concentrated mass of 400 kg.

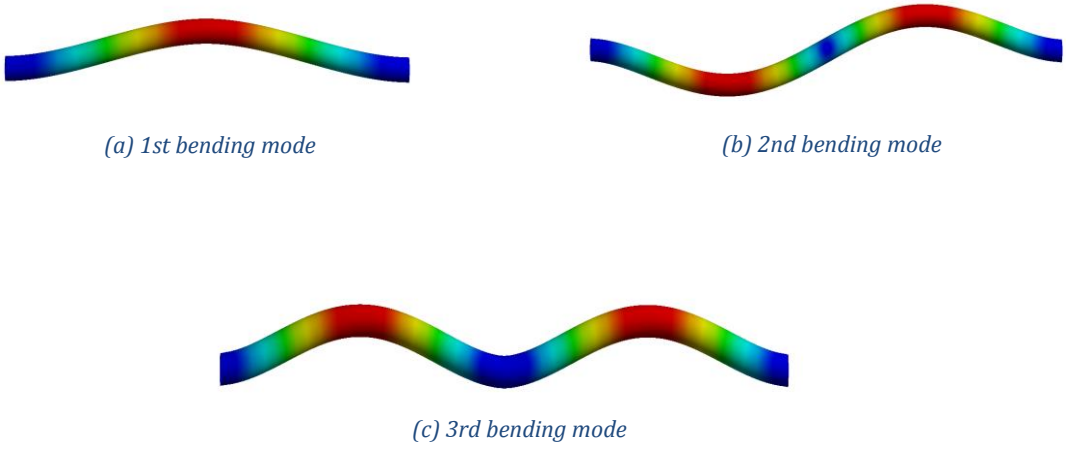

(a) 1st bending mode

(b) 2nd bending mode

(c) 3rd bending mode

Figure 4.1 – Illustration of the first three eigenmodes of pure bending for model 1

Table 4.1 - Eigenfrequencies and participation factors for the first three bending modes for computational model 1. The values are calculated for a concentrated mass of 400

Mode	Freq	Part.fact(x)	Part.fact(y)	Part.fact(z)	
1	9.8	19.7	-6.93	0.103E-3	Bending
3	116.5	2.43E-4	-1.15E-4	0.148E-1	Bending
6	167.3	2.94	-1.053	0.33E-4	Bending

4.1.2 Unwelded

Two allowable vibration velocity and frequency diagrams are presented for the unwelded case of pipe model 1. The first graph illustrates RMS vibration velocities for the first eigenmode with varying concentrated mass, presented in Figure 4.1.

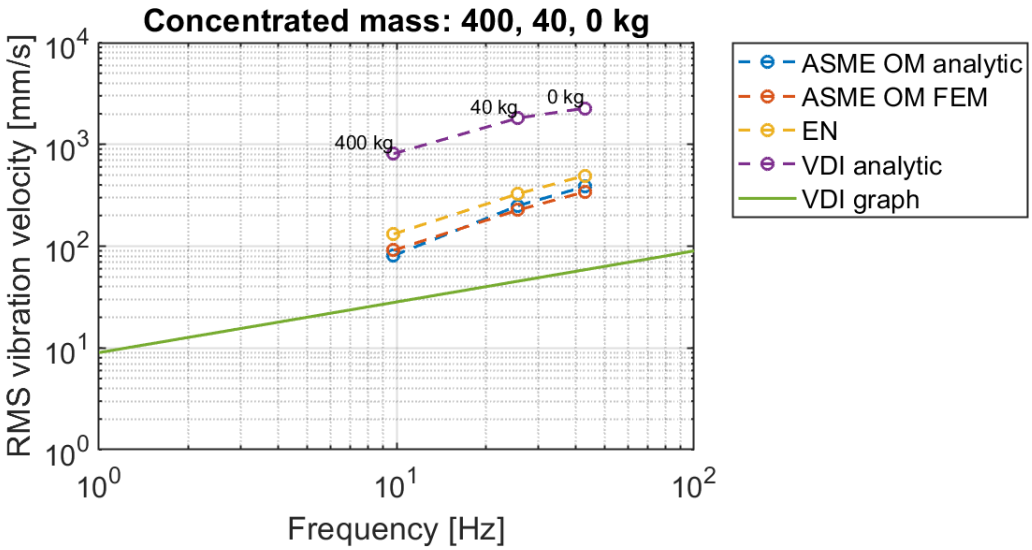

Figure 4.1 – Allowable RMS vibration velocity for 400, 40 and 0 kg concentrated mass restricted to the first eigenmode

The methods compared in Figure 4.1 show similar trends with increasing allowable RMS vibration velocity with increasing frequency. ASME OM analytic show higher allowable RMS vibration velocities compared to ASME OM FEM with increasing frequency.

Figure 4.2 illustrates RMS vibration velocity for the first three bending eigenmodes without a concentrated mass.

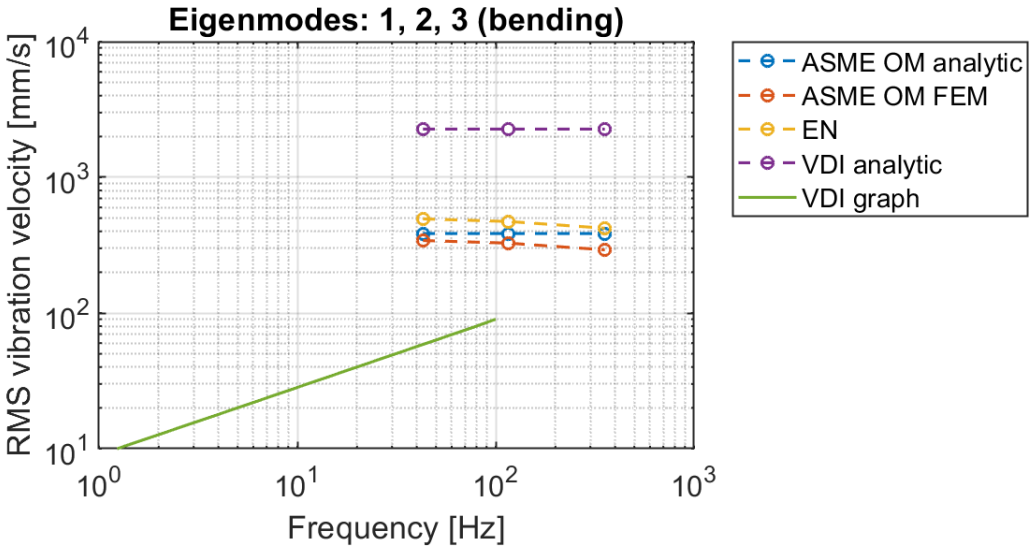

Figure 4.2 – Allowable RMS vibration velocity for the first three bending eigenmodes without a concentrated mass

All methods in Figure 4.2, except values from the VDI graph, have almost constant allowable RMS vibration velocities for varying eigenmodes. In other words, the allowable RMS vibration velocities has a very small frequency dependence for varying eigenmodes.

4.1.3 Welded

The allowable two vibration velocity and frequency diagrams for the unwelded case are recreated for the welded case of computational model 1. The first eigenmode with varying concentrated mass and a weld joint is presented in Figure 4.3.

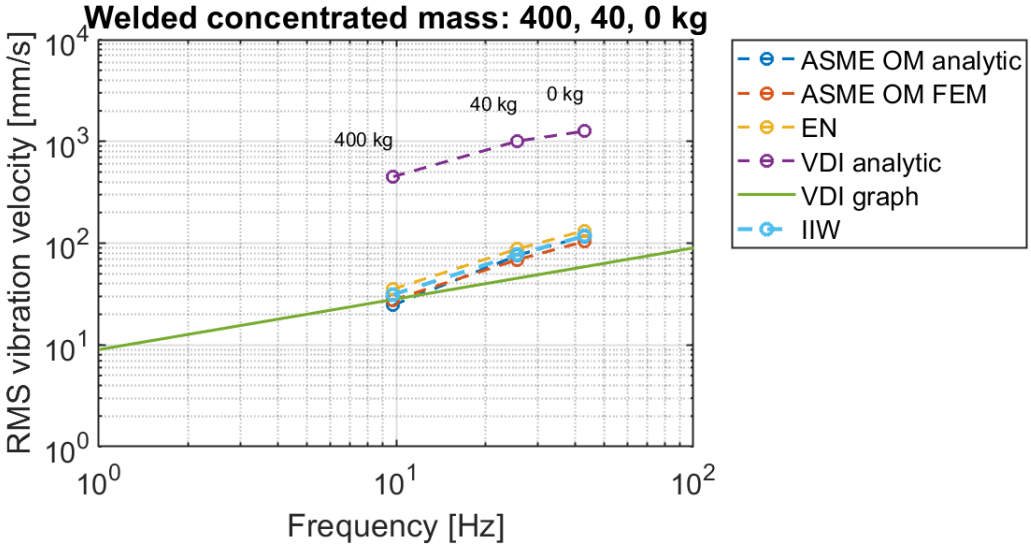

Figure 4.3 – Allowable RMS vibration velocity for 400, 40 and 0 kg concentrated mass restricted to the first eigenmode with a weld joint included

The same trends that can be seen for the unwelded pipe in Figure 4.1 is also depicted in Figure 4.3. The main difference is that allowable RMS vibration velocities are lower due to lower fatigue stress. ASME OM FEM and IIW are thus identical and shows the same behaviour as in Figure 4.3 and Figure 4.4. To avoid misunderstanding it should be noted that ASME OM FEM and IIW give identical results.

Allowable RMS vibration velocities for the first three bending eigenmodes for a welded pipe without concentrated mass is presented in Figure 4.4.

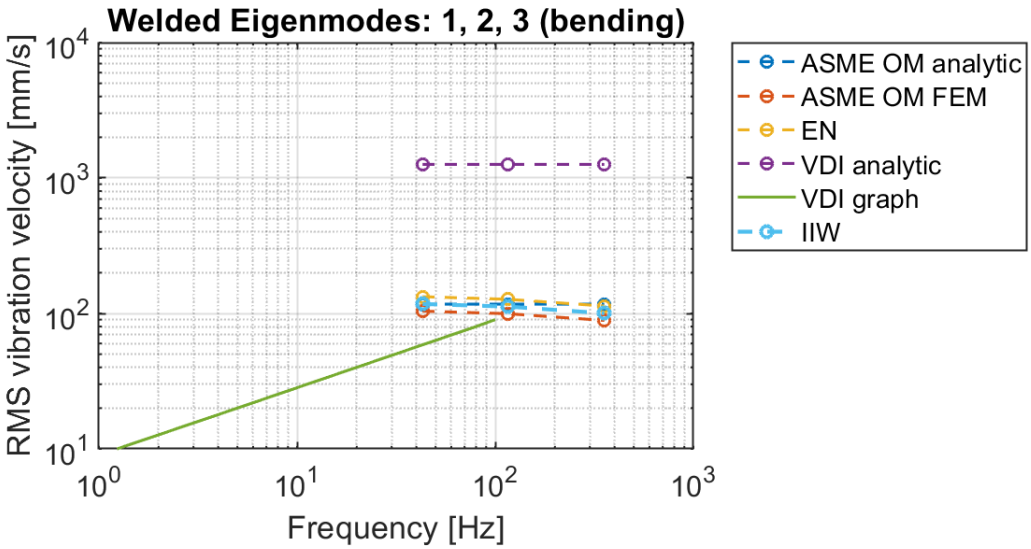

Figure 4.4 – Allowable RMS vibration velocity for the first three bending eigenmodes without a concentrated mass and a weld joint included

Same observations in Figure 4.3 applies to Figure 4.4. Allowable RMS vibration velocity levels have the same trend but are lower. Welded and unwelded allowable RMS vibration velocity levels are shown to have identical trends. The only difference is that welded allowable RMS vibration velocity levels are scaled down vertically due to lower fatigue stress for welded joints. With the inclusion of welds, allowable RMS vibration velocity levels do not give any additional information and are excluded from following diagrams. From Figure 4.3 and Figure 4.4 it can be concluded that all methods have identical trends and are therefore excluded in following diagrams in order to facilitate readability.

4.1.4 Eigenmodes for concentrated mass

From the previous diagrams, concentrated mass and eigenmodes are combined and the first three bending eigenmodes are compared in Figure 4.5 with increasing concentrated mass. In order to facilitate readability, Figure 4.5 only includes ASME OM FEM as well as values from the VDI graph. Neglected methods have identical trends but different allowable RMS vibration velocity levels.

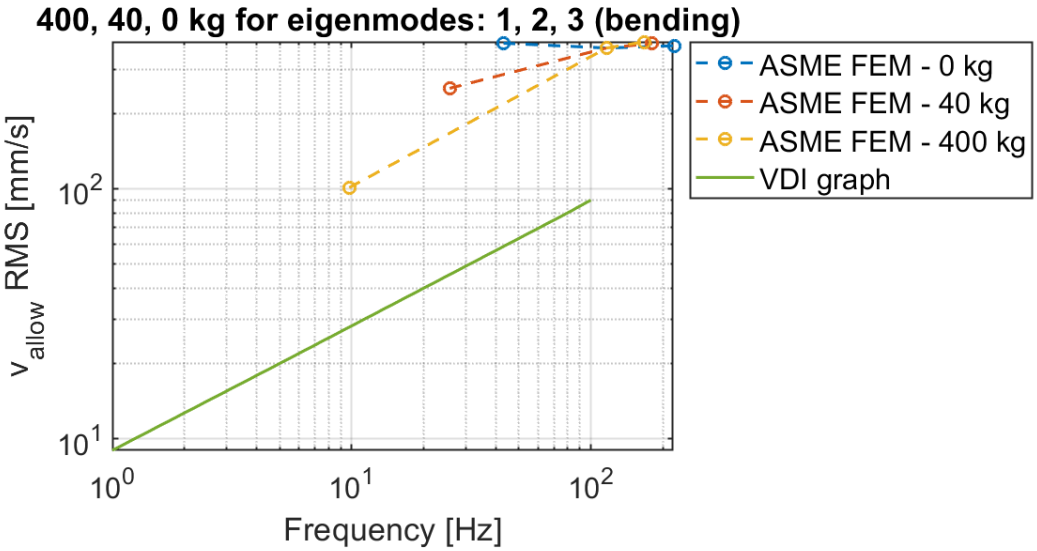

Figure 4.5 – Allowable RMS vibration velocity for varying eigenmodes with constant concentrated mass

From Figure 4.5, an increased frequency dependency of allowable RMS vibration velocity between eigenmodes is observed for higher concentrated mass.

4.2 Computational model 2

Results for the computational model 2 are divided into the same parts as in computational model 1, with the exception of exclusion of welds since the welds results are the same except for scaling. Mode shapes used for calculating allowable RMS vibration velocity are illustrated. The effects of concentrated mass and eigenmodes for a unwelded pipe and a combination of concentrated mass for varying eigenmodes will be analysed.

4.2.1 Vibration mode shapes

Eigenmodes used to create allowable RMS vibration velocity diagrams for computational model 2 are illustrated in Figure 4.6. Participation factors and eigenfrequencies for the eigenmodes are summarized in Table 4.2. A concentrated mass of 10 kg was used.

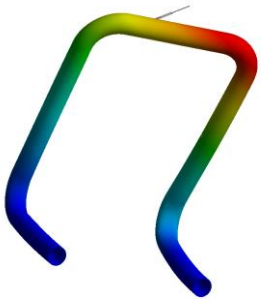

(a) 1st vibration mode

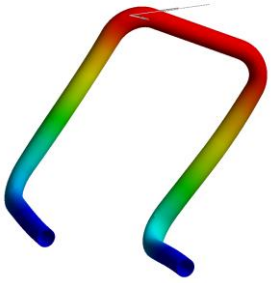

(b) 2nd vibration mode

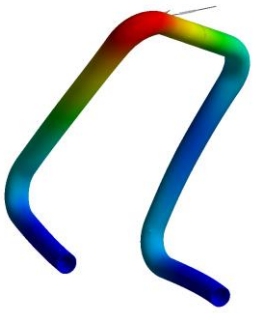

(c) 3rd vibration mode

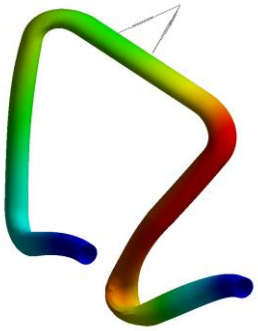

(d) 4th vibration mode

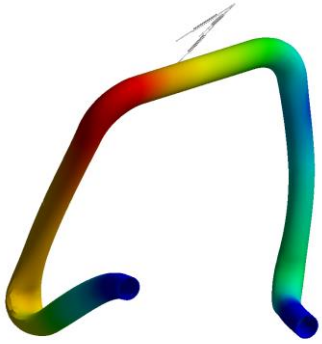

(e) 5th vibration mode

Figure 4.6 - Illustration of the first five eigenmodes for model 2

From Figure 4.6 it is evident that it is difficult to distinguish if the vibration is pure bending which can affect the maximum stress used to calculate allowable RMS vibration velocity levels.

Table 4.2 - Eigenfrequencies and participation factors for the investigated vibration modes belonging to computational model 2. Contour plots are extracted from ANSYS.

Mode	Freq	Part.fact(x)	Part.fact(y)	Part.fact(z)
1	34.8	127.25	-48.723	7.688
2	48.018	8.996	38.634	133.68
3	62.654	20.217	23.332	-10.678
4	85.756	36.562	118.67	-53.50
5	132.618	3.050	71.244	23.28

4.2.2 Unwelded

Two allowable vibration velocity and frequency diagrams are presented for the unwelded case of computational model 2. Figure 4.7 illustrate allowable RMS vibration velocities for the first eigenmode with varying concentrated mass. All methods exhibits same trends with the only difference that the values are scaled with the same factor as in Figure 4.1 and Figure 4.2. Including more methods will therefore not provide more information than Figure 4.7 and is thus neglected.

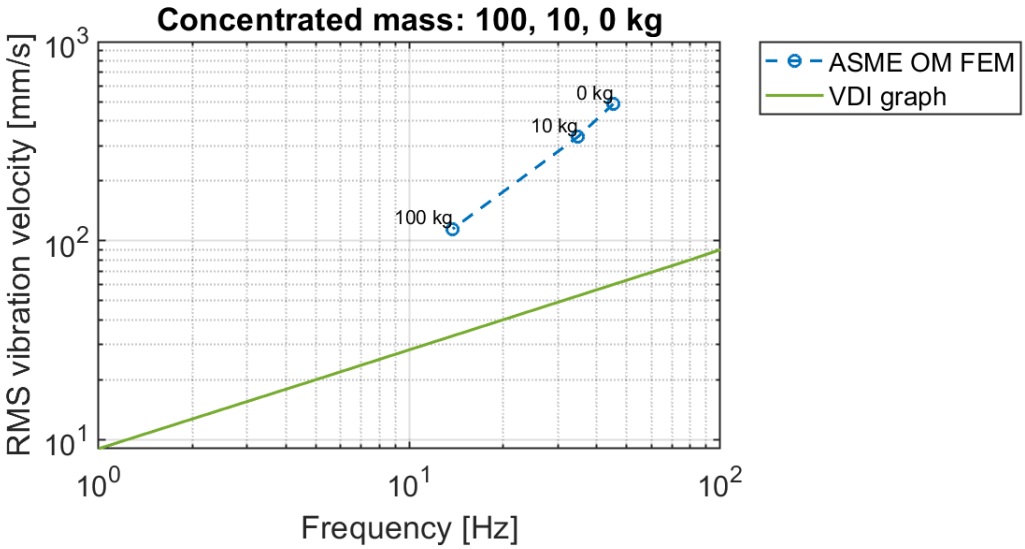

Figure 4.7 – Allowable RMS vibration velocity for 100, 10 and 0 kg concentrated mass restricted to the first eigenmode

The methods compared in Figure 4.7 have similar trends as for computational model 1 with increasing allowable RMS vibration velocity with increasing frequency.

Figure 4.8 illustrate RMS vibration velocities for the first five eigenmodes without a concentrated mass.

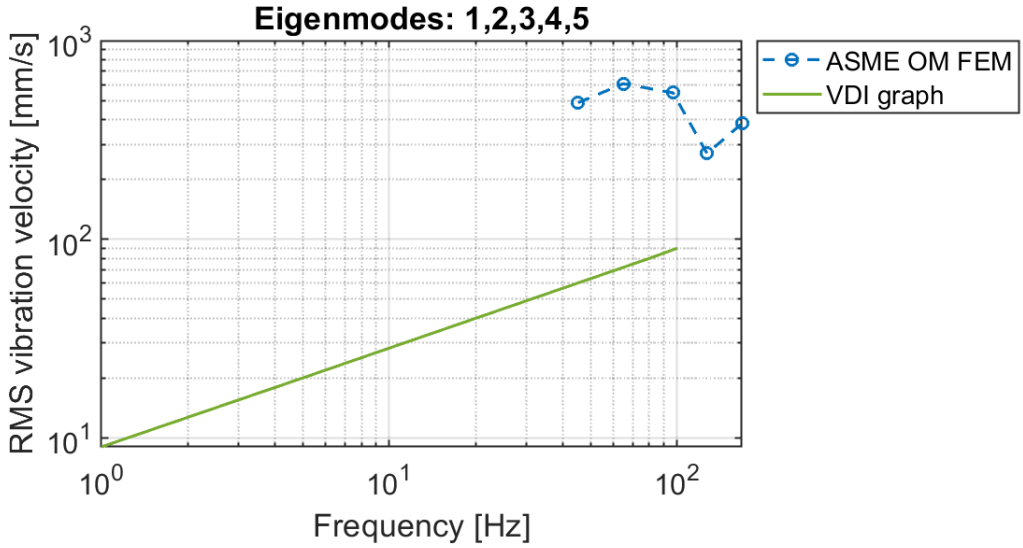

Figure 4.8 – Allowable RMS vibration velocity for the first five eigenmodes without a concentrated mass

The methods in Figure 4.8 show a decrease in allowable RMS vibration velocity with increasing eigenfrequencies, unlike the case for computational model 1 where the slope is positive.

4.2.3 Eigenmodes for concentrated mass

In previous diagrams, concentrated mass and eigenmodes are combined and the first five eigenmodes are compared in Figure 4.9 with increasing concentrated mass. To improve readability, only values from ASME OM FEM and ASME OM analytical and VDI graph are included. Neglected methods have the same trend but different allowable RMS vibration velocity levels.

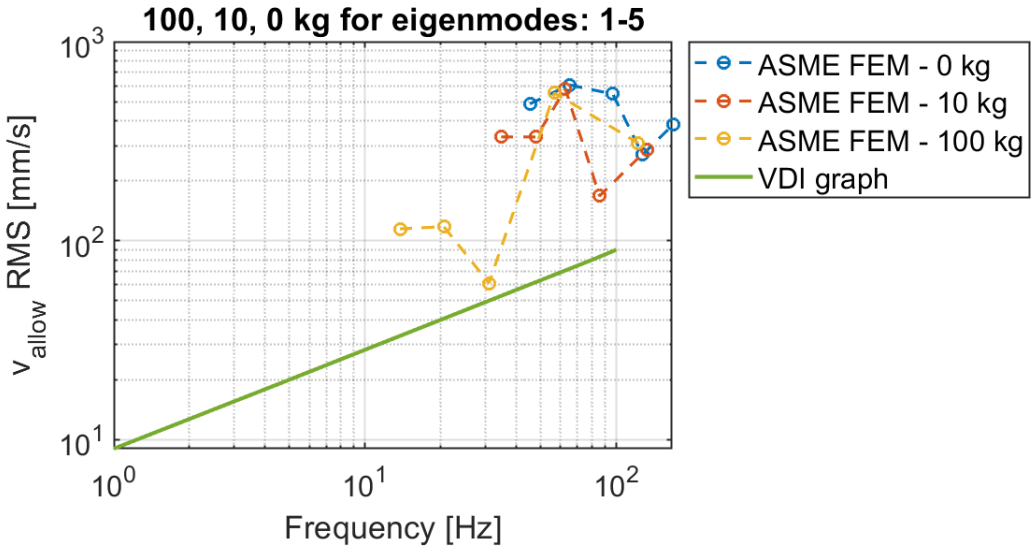

Figure 4.9 - Allowable RMS vibration velocity for varying eigenmodes with constant concentrated mass

Allowable RMS vibration velocities in Figure 4.9 becomes irregular for higher eigenmodes and increasing concentrated mass, unlike the case for computational model 1 where a linear increase of allowable RMS vibration velocity for higher concentrated mass and eigenmodes was observed.

4.3 Computational model 3

The results for computational model 3 was obtained by performing modal analysis and harmonic response analysis, where an acceleration amplitude is prescribed over the entire model in y-direction and the forcing frequency is varied over a frequency range from $0 - 100$ Hz. Since mode superposition is used the results are linear and the acceleration amplitude have limited importance implying that the results can be scaled.

4.3.1 Vibration eigenmodes

Some of the eigenmodes used to establish allowable RMS vibration velocities for computational model 3 are illustrated in Figure 4.10. Participation factors and eigenfrequencies for eigenmodes are summarized in Table 4.2 where a concentrated mass of 200 kg is used. The position of the mass can be seen in Figure 3.3.

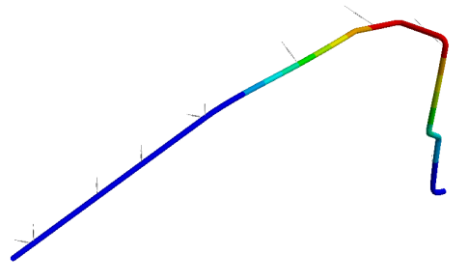

(a) 1st vibration mode

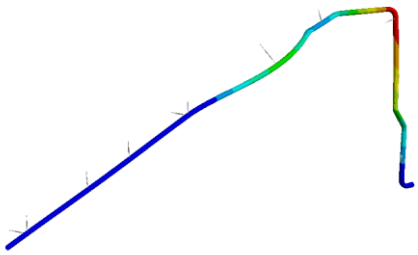

(b) 3rd vibration mode

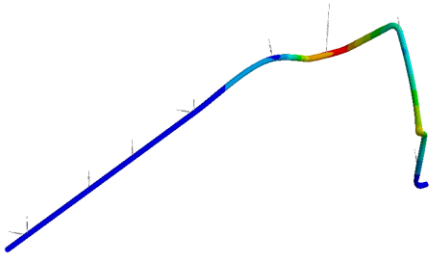

(c) 4th vibration mode

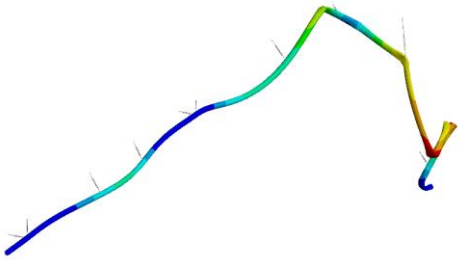

(c) 9th vibration mode

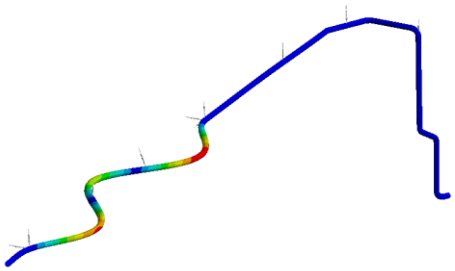

(d)13th vibration mode

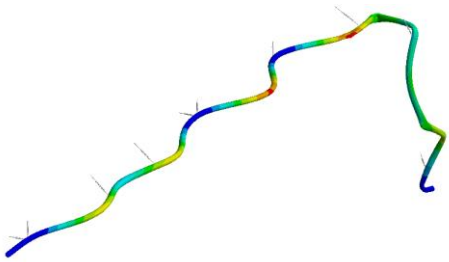

(e) 18th vibration mode

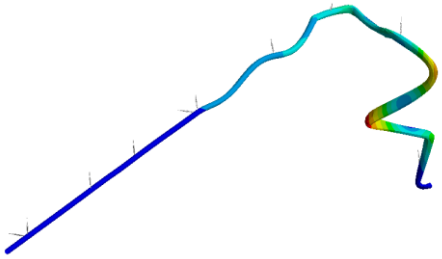

(f) 21st vibration mode

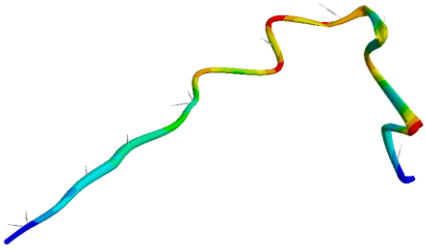

(g) 23rd vibration mode

Figure 4.10 - Illustration of a selection of eigenmodes for model 3

From Figure 4.10 it is evident that it is difficult to distinguish if the vibration is purely bending, as was the case for computational model 2. However, some mode shapes with pure bending such as vibration mode 13 (e) can be identified.

Table 4.3 - Eigenfrequencies and participation factors for the illustrated vibration modes belonging to computational model 3.

Mode	Freq	Part.fact(x)	Part.fact(y)	Part.fact(z)
1	1.07	3.66	39.778	1.122
3	2.92	25.10	-9.674	-8.759
4	4.46	1.19	-11.236	19.051
9	10.29	11.43	-0.358	20.559
13	15.62	-0.34E-1	14.973	-0.315E-1
18	25.37	-0.860E-1	-0.420E-2	35.290
21	33.71	21.131	-1.359	3.162
23	35.30	-38.683	-2.555	-0.208

4.3.2 Modal analysis

Two allowable RMS vibration velocity and frequency diagrams are presented for the unwelded case of computational model 3. The first diagram illustrates allowable RMS vibration velocity for a bending eigenmode with varying concentrated mass, depicted in Figure 4.11. Only ASME OM FEM and VDI graph are included to improve readability. Neglected methods have the same trend but different allowable RMS vibration velocities.

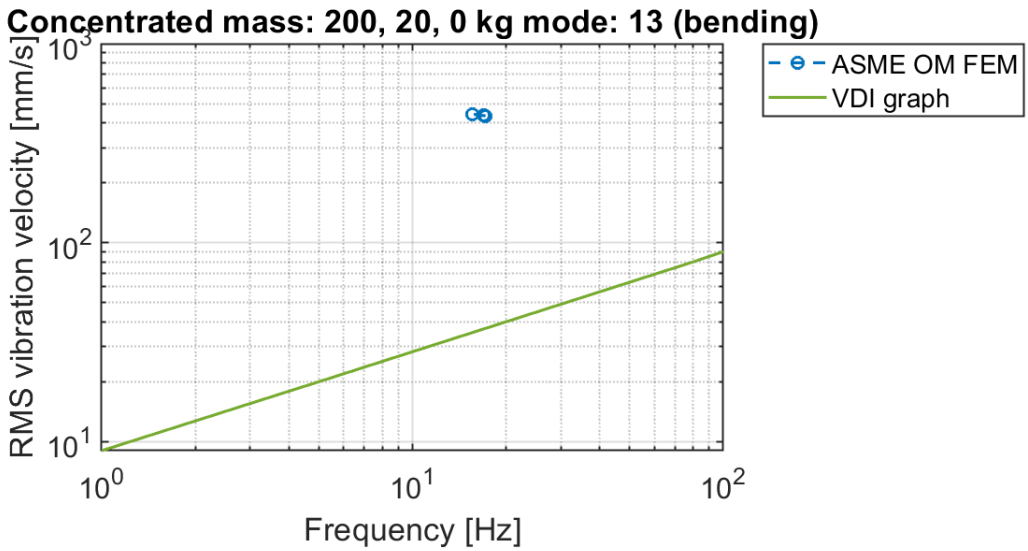

Figure 4.11 – Allowable RMS vibration velocity for 200, 20 and 0 kg concentrated mass restricted to bending eigenmode illustrated in Figure 4.10d

The methods in Figure 4.11 have decreasing allowable RMS vibration velocity for increasing concentrated mass.

The second diagram illustrates allowable RMS vibration velocities for eigenmodes with a frequency range of 0 to 50 Hz, without a concentrated mass, depicted in Figure 4.12. It should be pointed out that results for 20 and 0 kg added concentrated mass coincide.

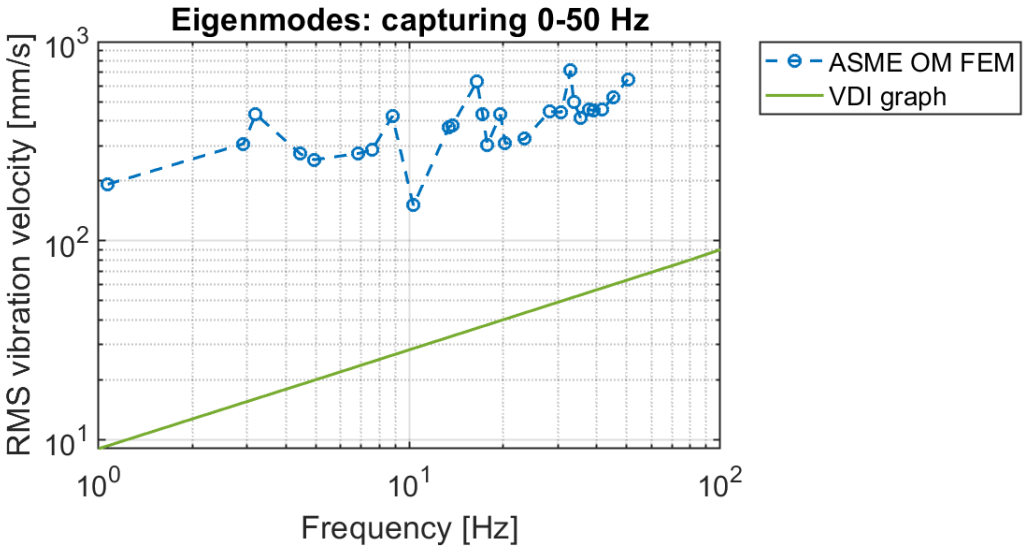

Figure 4.12 – Allowable RMS vibration velocity for eigenmodes capturing eigenfrequencies up to 50 Hz without added concentrated mass

From Figure 4.12, an erratic behaviour of allowable RMS vibration velocities can be observed. ASME OM FEM is shown to have considerably higher allowable RMS vibration velocities compared to VDI.

4.3.2.1 Eigenmodes for concentrated mass

From previous diagrams, concentrated mass and eigenmodes are combined and the eigenmodes from a frequency range of up to 50 Hz are compared in Figure 4.13 with increasing concentrated mass. To improve readability, only values for ASME OM FEM and VDI graph are included. Neglected methods have the same trend but different allowable RMS vibration velocities.

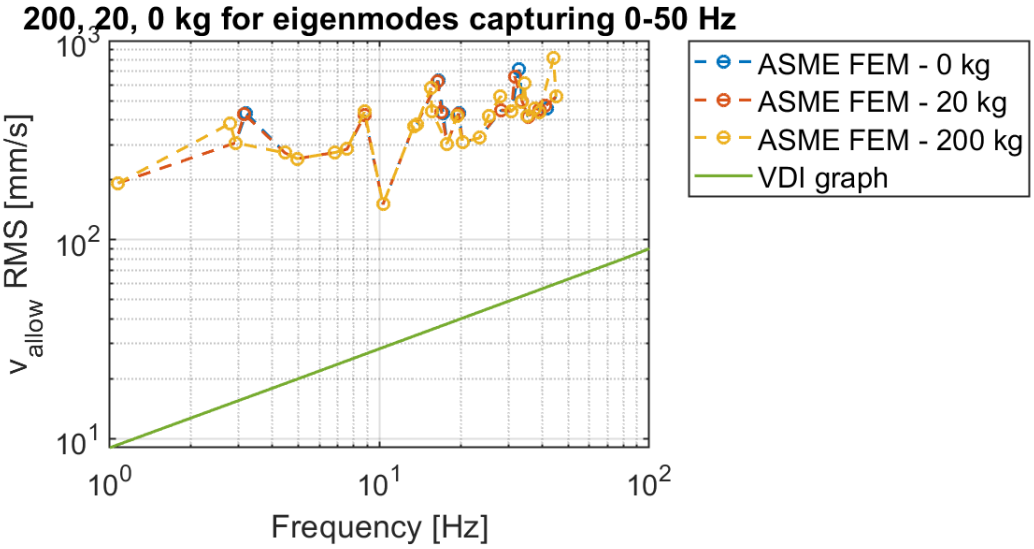

Figure 4.13 - Allowable RMS vibration velocity for eigenmodes capturing 0 to 50 Hz with increasing concentrated mass of model 3

The allowable RMS vibration velocities in Figure 4.13 show a similar behaviour for different concentrated masses. It should be pointed out that ASME FEM 0 kg and ASME FEM 20 kg coincide in Figure 4.13.

4.3.3 Harmonic response analysis

Response from harmonic analysis at a given frequency in piping system subjected to a uniform acceleration amplitude on computational model 3 with 200 kg concentrated mass is depicted in Figure 4.14. All eigenmodes in the simulation are included, not only the ones depicted in Figure 4.10.

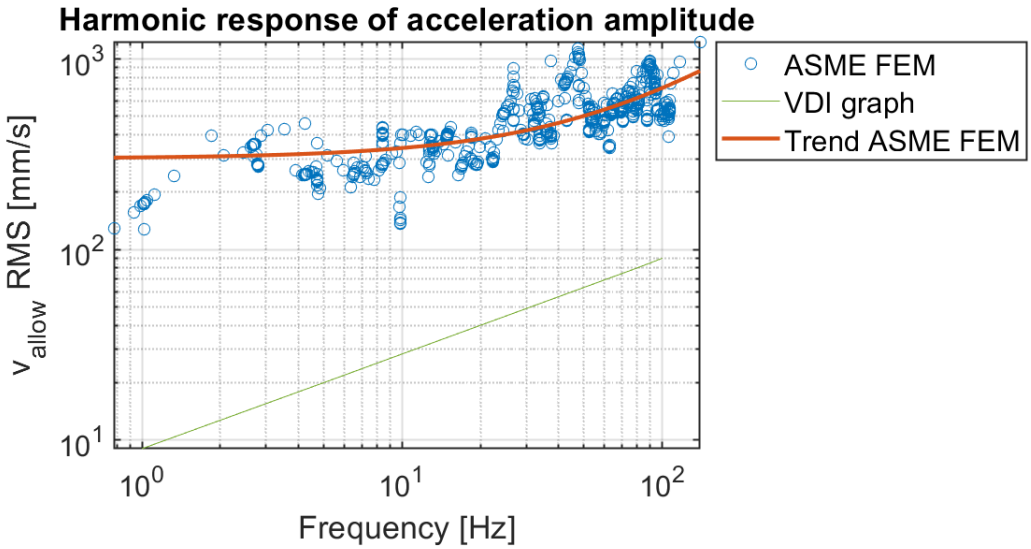

Figure 4.14 – Response of allowable RMS vibration velocity to harmonic acceleration amplitude for model 3

From Figure 4.14, an erratic behaviour of the allowable RMS vibration velocity can be observed from the harmonic response analysis where lowest allowable RMS vibration velocities corresponds to excitation of eigenfrequencies. Allowable RMS vibration velocities in Figure 4.14 are observed to be similar to allowable RMS vibration velocities from modal synthesis, Figure 4.13. Since mode superposition is used for harmonic response analysis, frequencies excited between eigenmodes will result in a linear combination of respective eigenmodes. Similar allowable RMS vibration velocity trends from harmonic response analysis indicates that the results indeed are super positioned values from modal analysis. A selection of the lowest allowable RMS vibration velocities from Figure 4.14 are illustrated in Figure 7.1, Appendix B . A brief sensitivity analysis on spring stiffness, wall thickness and pipe density together with welded harmonic response result are included in Appendix B .

5 Discussion

Allowable RMS vibration velocities are greatly influenced by added concentrated masses and presence of welds. For computational model 1, allowable RMS vibration velocities for all methods are linearly increasing with the increasing frequency that is result of reducing concentrated mass, with the exception of the first eigenmode. From eigenmode analysis, without concentrated mass it is observed that computational model 1 shows constant allowable RMS vibration velocity levels with increasing eigenfrequencies but that is not the case for the other two computational models. The reason for this can be that increasing eigenfrequencies with higher eigenmodes is counteracted by changing displacement and stress intensity. Therefore, geometry dependent eigenmodes will affect the trend of allowable RMS vibration velocities. In other words, increasing geometry complexity will result in complex eigenmodes which in turn lead to allowable RMS vibration velocities with fluctuating frequency dependence. Analysis of a combination of decreasing concentrated mass and varying eigenmodes show increasing frequency dependence between eigenmodes with increased concentrated mass for the first two computational models.

Lower allowable RMS vibration velocities are observed for welded pipes which is logical since presence of welds gives the lower fatigue strength specified by welded design fatigue curves or correction factors. Hence, all methods calculating allowable RMS vibration velocities from welded design fatigue curves are scaled accordingly.

Differences in allowable RMS vibration velocities between methods may be explained by the different probability of failure for their corresponding design fatigue curves. Welded fatigue data from EN 13445 represent a probability of failure of 0.14% while fatigue data from IIW represent a probability of failure of 5%. Other methods such as ASME and KTA provides vague explanations about what probability of failure their fatigue data represent, making it difficult to do a comparative study.

All methods provide similar allowable RMS vibration velocities where the difference lie in the correction factors and fatigue data. Without experimental data or measurements of actual fatigue cases in the piping systems, it is difficult to determine the most accurate method. However, from comparison in Figure 4.3 it is evident that screening method for VDI is very conservative in terms of allowable RMS vibration velocity. While, EN, IIW and ASME OM FEM are slightly less conservative than values from VDI graph. Allowable RMS vibration velocities for ASME OM FEM and IIW are almost identical which may indicate a similar level of conservatism.

With increasing model complexity, it becomes increasingly difficult to identify eigenmodes with pure bending, since allowable RMS vibration velocity levels should refer to fatigue, which is often based on bending stress. It is thus important that the stress used to calculate allowable RMS vibration velocities represent bending stress.

When performing modal analysis on a free undamped system only modal properties are obtained. In order to obtain real physical vibration amplitudes, harmonic response analysis should be performed by knowing the actual size of the excitation, this could be in the form of a known acceleration signal from measurements together with damping properties. Because harmonic response analysis is performed on an undamped system,

the results show modes with very large displacement amplitudes at low frequencies which are clearly not physical. By including damping, the vibration amplitudes may give a more physical representation of the system. However, this should not affect the allowable RMS vibration velocity since the stresses should decrease as well as the vibration amplitudes resulting in the same allowable RMS vibration velocity.

It has been assumed that the oscillations are harmonic which may not be a correct representation of a real system, where the response can be of transient character. The difference for non-harmonic oscillations may be that displacements vary in time and harmonic oscillations can therefore be seen as less conservative values for allowable RMS vibration velocity levels.

Eigenmodes have been sorted based on modes with highest modal participation factor to evaluate critical modes, i.e. modes with low allowable RMS vibration velocities. Although eigenmodes with high participation factor are shown to provide low allowable RMS vibration velocities this may not be a sufficient condition to sort eigenmodes. Eigenmodes with low participation factor may provide low allowable RMS vibration velocity levels, it is therefore important to expand the analysis by also looking at modes with low participation factors.

6 Conclusion

The purpose of this thesis was to calculate allowable RMS vibration velocity levels for piping configurations with different methods. Evaluation of the different methods were evaluated for three different computational models with increasing complexity. Allowable RMS vibration velocities were assessed and quantified by varying concentrated mass and geometric properties. Eigenfrequencies and eigenmodes were obtained by performing modal analysis for all computational models. In order to obtain actual displacement and stress amplitudes, an excitation load in the form of a prescribed acceleration amplitude was applied to computational model 3 over a forcing frequency range up to 100 Hz.

Results show that all models have a linear, or close to linear relation between allowable RMS vibration velocity and frequency, this relation exist for all methods. When concentrated mass were excluded, results show that all methods exhibit very little frequency dependence between eigenmodes for computational model 1. However, when concentrated mass was included, computational model 1 show increasing frequency dependence between eigenmodes with an increase in concentrated mass. Frequency dependence between eigenmodes for computational model 2 and computational model 3 show a more fluctuating behaviour. Computational model 2 and computational model 3 show that higher model complexity makes it difficult to distinguish pure bending modes.

7 References

Agrawal, R., Uddanwadiker, R & Padole, P. (2014): *Low Cycle Fatigue Life Prediction.* International Journal of Emerging Research and Technology. Volume 2, Issue 4. pp. 5-15.

Ahmed, A. S. (2019): Theory of Vibrations. An Introduction, Third Edition. Springer International Publishing AG, New York, USA, pp.375.

ANSYS (2019): ANSYS 2019 R2.Manual Mechanical APDL Theory reference, ANSYS, Inc., Canonsburg, PA.

ASME (2002). Part 3 – Requirements for Preoperational and Initial Start-up Vibration Testing of Nuclear Power Plant Piping Systems, in: ASME OMb-S/G-2002 addenda to ASME OM-S/G-2000 Standards and Guides for Operation and Maintenance of Nuclear Power Plants, American Society of Mechanical Engineers, New York, NY, pp. 19-64.

ASME BPVC (2015). Boiler and Pressure Vessel Code, American Society of Mechanical Engineers, New York, NY, p.

ASME-OM (2015). Operation and Maintenance of Nuclear Power Plants, in: ASME OM-2015, American Society of Mechanical Engineers, New York, NY.

ASM International (2008): *Elements of Metallurgy and Engineering Alloys*, Chapter 14 - Fatigue. ASM International, Materials Park, Ohio, USA, p. 264.

Banerjee, B., Chen, J., Das, R . (2013): Comparison of ANSYS elements SHELL181 and SOLSH190.

Clough, R.W. & Penzien, J. (2003): Dynamics of Structures, Third edition, Computers & Structures, Inc., Berkeley, CA, 730 p.

Comsol. (2018): Multiphysics cyclopedia – eigenfrequency analysis , Comsol, Inc., Burlington, MA. https://www.comsol.se/multiphysics/eigenfrequency-analysis. (Retrieved: 2019-11-05)

Comsol. (2018): Multiphysics cyclopedia – Material Fatigue, Comsol, Inc., Burlington, MA.

https://www.comsol.se/multiphysics/material-fatigue .(Retrieved:2019-11-28)

Craig, R.R. & Kurdila, J.A (2006): Fundamentals of Structural Dynamics, Second Edition, John Wiley & Sons, Inc., Hoboken., NJ, USA, 728 p.

Cruz, M., Lopez, O.A (1996): NUMBER OF MODES FOR THE SEISMIC DESIGN OF BUILDINGS. Earthquake engineering & Structural Dynamics. Vol. 25, pp. 838-855.

Dowling, N.E. (2013): Mechanical Behavior of Materials, Fourth Edition. Pearson Education Limited, Essex, UK, pp. 954.

Energiforsk (2017). Energiforsk report 2017:451, Pipe vibrations in nuclear applications, Energiforsk, Stockholm, p.95.

European Union (1993): Eurocode 3: Design of steel structures – Part 1-9 Fatigue.

Fomin, V., Kostarev, V. & Reinsch, K. (2001). Elimination of Chernobyl NPP unit 3 power output limitation associated with high main steam piping flow induced vibration, Proceedings of the 16th International Conference on Structural Mechanics in Reactor Technology, Washington, DC, pp. 1375-1383.

Haukass, T. (2019): Oscillating mass., The University of British Columbia, Vancouver, 11 p. http://civil-terje.sites.olt.ubc.ca/files/2019/06/Oscillating-Mass.pdf (Retrieved: 2019-11-19)

He, Jimin., Fu, Zhi-Fang . (2001): Modal Analysis. Butterworth/Heinemann, Oxford, United Kingdom.

IAEA (2016): Operating Experience with Nuclear Power Stations in Member States in 2015, International Atomic Energy Agency, Vienna, p.1540

IIW (2008). IIW-1823-07 Recommendations for fatigue design of welded joints and components, International Institute of Welding, Paris.

Irvine, T. (2011): Effective modal mass & modal participation factors. http://www.vibrationdata.com/tutorials2/ModalMass.pdf (Retrieved: 2019-11-05)

Kostarev, V., Tuomas, A. & Reinsch, K. (2007). Resolving of steam and feed-water piping vibration matter at Loviisa NPP, Transactions of the 19th International Conference on Structural Mechanics in Reactor Technology (SMiRT 19) J, pp. 12-17.

Kostarev, V.V., Berkovski, A.M. & Schukin, A.J. (1999). Upgrading of dynamic reliability and life extension of piping by means of high viscous damper technology, pp. 155-162.

KTA (2013). KTA 3211.2:2013-11 Pressure and Activity Retaining Components of Systems Outside the Primary Circuit; Part 2: Design and Analysis, Kerntechnischer Ausschuss, Neuwied.

Larsson T. (2009): Fatigue assessment of riveted bridges. Ph.D. Thesis. Department of Civil and Environmental Engineering, Luleå University of Technology, Publication no. 01:2, Göteborg, Sweden, 2001, 152 pp.

Möller, P. (2018): FEM – Compiled lecture notes, Gothenburg, Sweden. p. 143.

Ottosen, N., Petersson, H. (1992): Introduction to the Finite element method, first edition, Prentice Hall Europe, Edinburgh Gate Harlow, Essex. pp.410.

Piersol, A., Harris, C. (2002): Shock and Vibration Handbook, fifth edition. McGRAW-HILL, Inc., US.

Reddy, J. N. (2008): An Introduction to Continuum Mechanics with applications. Cambridge University Press, Cambridge, United Kingdom.

Seligmann, D. & Guillou, J. (1995). Flow induced vibrations in a PWR piping system, Électricité de France, Paris, p.10

Siemens simcenter (2019): Root Mean Square (RMS) and Overall Level.

https://community.sw.siemens.com/s/article/root-mean-square-rms-and-overall-level (Retrieved: 2019-12-13)

Swedish Standards Institute, SIS. (2009), SS-EN 13445-3:2009 Unfired pressure vessels – Part 3: Design. 2nd edition, Stockholm: SIS Förlag AB.

VDI (2004). VDI 3842:2004-6 Vibrations in piping systems, Verein Deutscher Ingenieure, Düsseldorf, p.87

Wang. E. (2006): Thin wall-structure simulation. https://www.ansys.com/-/media/Ansys/corporate/resourcelibrary/conference-paper/2006-Int-ANSYS-Conf-22.pdf (Retrieved: 2019-09-30)

Appendix A Summary of fatigue data

Table 7.1 - Material type and corresponding fatigue endurance limit from each industry standard used to evaluate allowable RMS vibration velocity

	Material	$S_{A,end}$ [MPa]
ASME	Carbon steel	86
	Austenitic steel	93,7
EN	Unwelded ferritic steel/austenitic	152,25
	Welded ferritic steel/austenitic	23
VDI - KTA	Ferritic steel	86,2
	Austenitic steel	127
IIW	Unwelded Steel	60
	Welded Steel	20,5

Appendix B Results from harmonic response analysis

Figure 7.1 illustrates a selection of frequencies with lowest allowable RMS vibration velocity that matches eigenfrequencies from modal analysis of model 3.

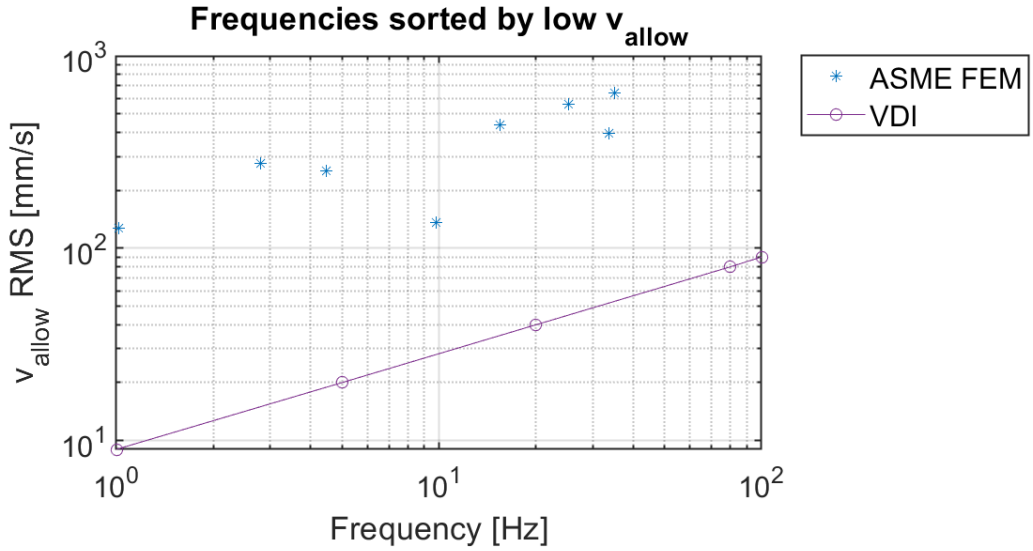

Figure 7.1 – Frequencies chosen by low allowable RMS vibration velocity, for model 3

B.1 Welded

The response from harmonic analysis on model 3 including a weld joint is presented in Figure 7.2.

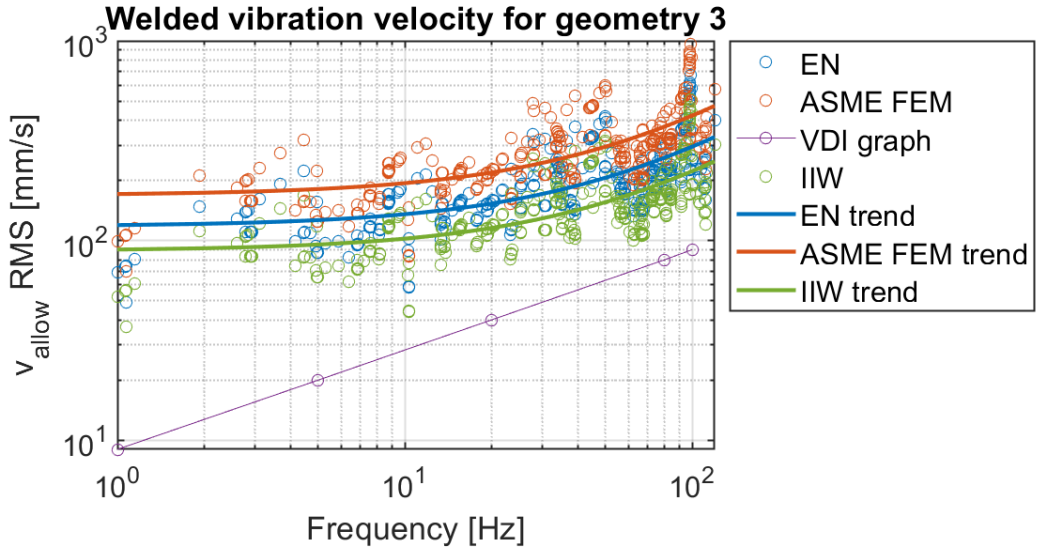

Figure 7.2 – Allowable RMS vibration velocity for harmonic response of model 3 including a weld joint

Figure 7.3 illustrates a selection of frequencies with lowest allowable vibration velocity that matches eigenfrequencies from modal analysis of model 3 including a weld joint.

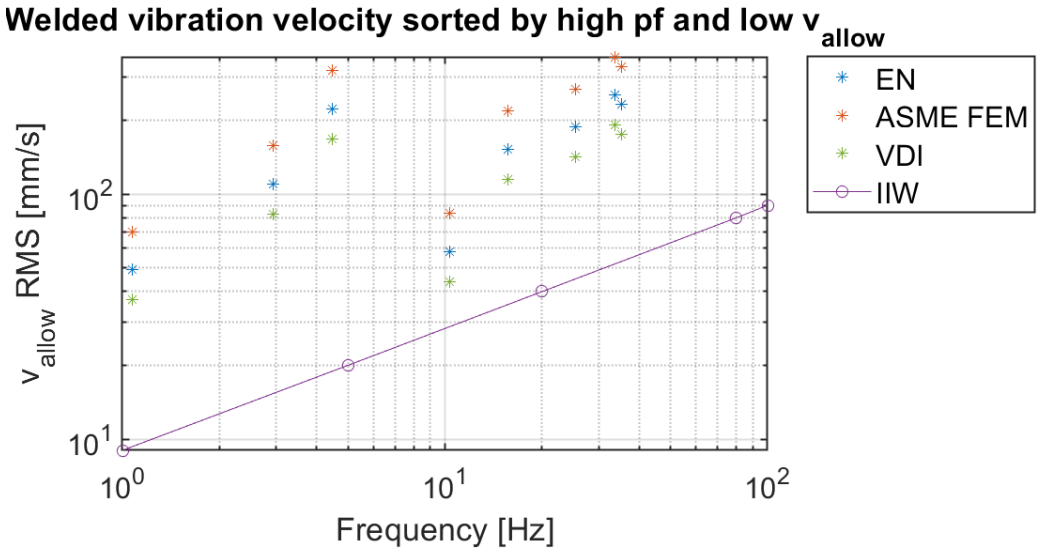

Figure 7.3 – Frequencies chosen by low allowable RMS vibration velocity, for model 3 including a weld joint

B.2 Sensitivity analysis

The response from harmonic analysis on model 3 with a 10% increase to spring stiffness is presented in Figure 7.4.

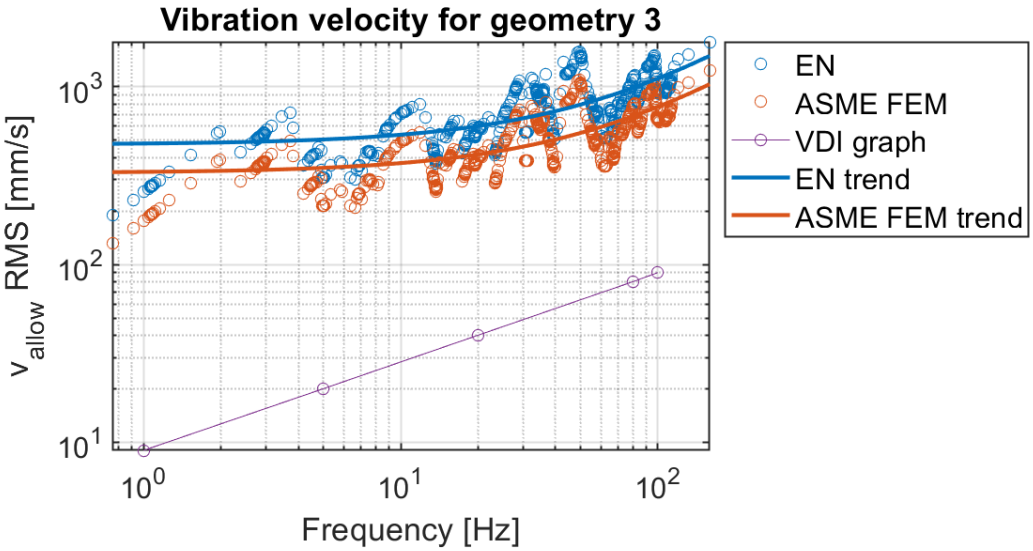

Figure 7.4 – Allowable RMS vibration velocity for model 3 with 10% increased spring stiffness

Figure 7.5 illustrates a selection of frequencies with lowest allowable RMS vibration velocity from the harmonic response analysis of 10% increased spring stiffness.

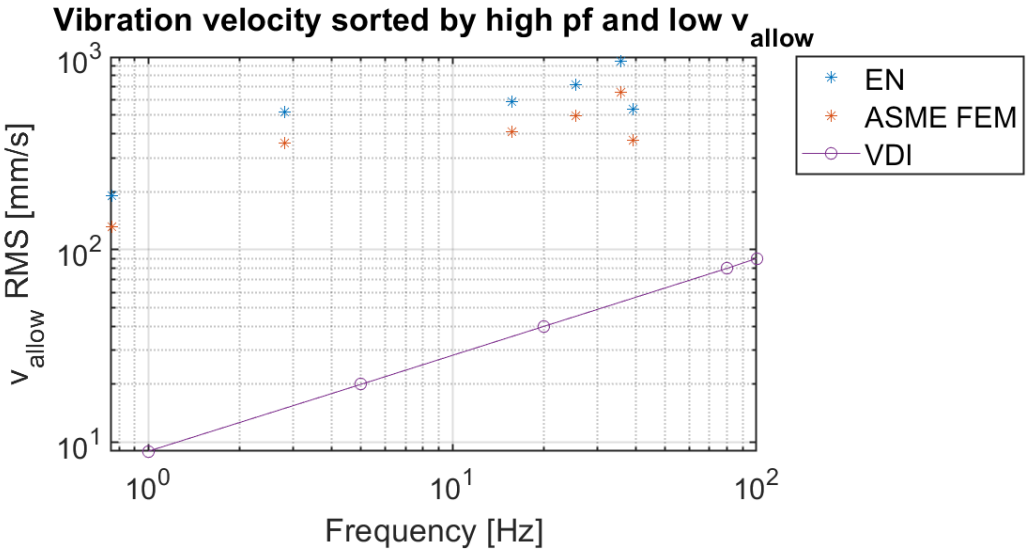

Figure 7.5 – Allowable RMS vibration velocity of chosen frequencies for FE model 3 with 10% increased spring stiffness

The response from harmonic analysis on model 3 with a 50% increase to wall thickness is presented in Figure 7.6.

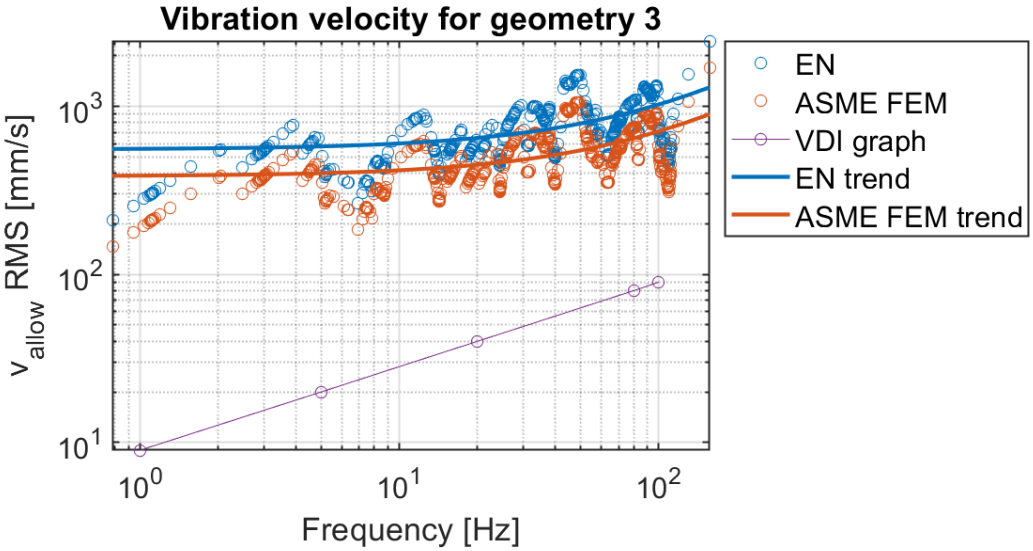

Figure 7.6 – Allowable RMS vibration velocity for model 3 with 50% increased pipe wall thickness

Figure 7.7 illustrates a selection of frequencies with lowest allowable RMS vibration velocity from the harmonic response analysis of 10% increased spring stiffness.

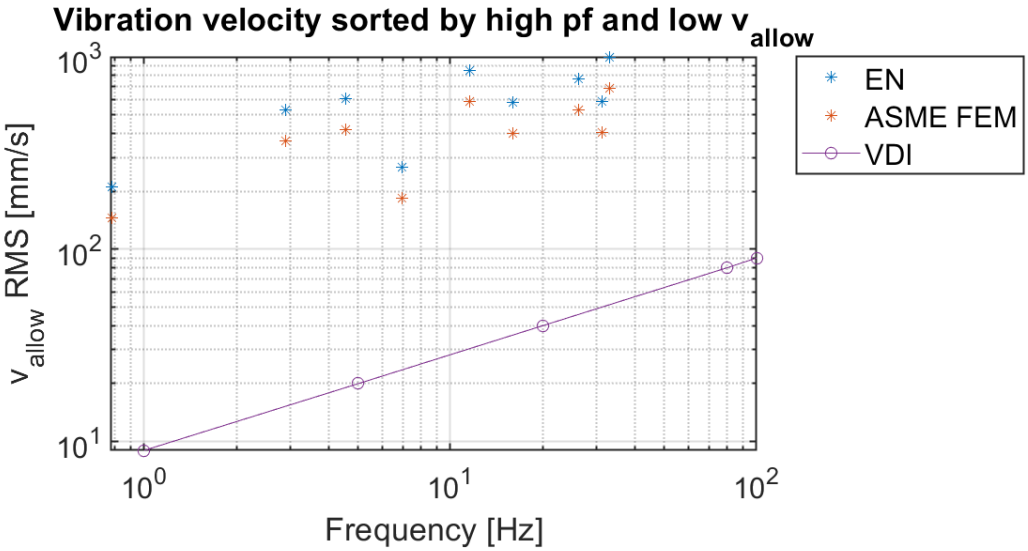

Figure 7.7 – Allowable RMS vibration velocity of chosen frequencies for FE model 3 with 50% increased pipe wall thickness

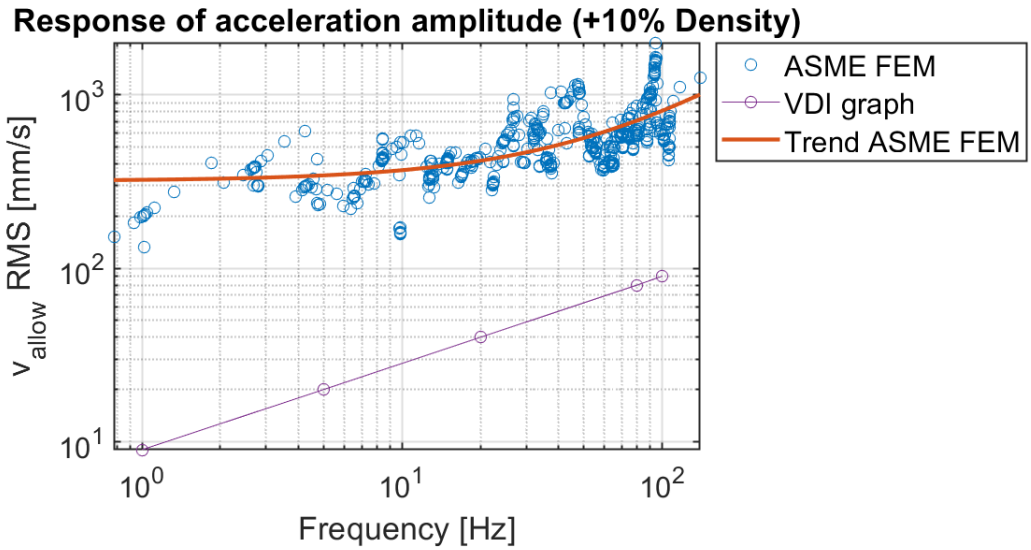

Figure 7.8 - Response of allowable RMS vibration velocity to harmonic acceleration amplitude with 10% increased density for model 3

Appendix C Design Fatigue Data

Table I-9.1
Tabulated Values of S_a, ksi (MPa), From Figures I-9.1 and I-9.1M

Number of Cycles [Note (1)]	UTS 115 ksi to 130 ksi (UTS 793 MPa to 896 MPa)	UTS ≤ 80 ksi (UTS ≤ 552 MPa)
1E1	420 (2 896)	580 (3 999)
2E1	320 (2 206)	410 (2 827)
5E1	230 (1 586)	275 (1 896)
1E2	175 (1 207)	205 (1 413)
2E2	135 (931)	155 (1 069)
5E2	100 (689)	105 (724)
1E3	78 (538)	83 (572)
2E3	62 (427)	64 (441)
5E3	49 (338)	48 (331)
1E4	44 (303)	38 (262)
1.2E4 [Note (2)]	43 (296)	
2E4	36 (248)	31 (214)
5E4	29 (200)	23 (159)
1E5	26 (179)	20 (138)
2E5	24 (165)	16.5 (114)
5E5	22 (152)	13.5 (93)
1E6	20 (138)	12.5 (86)
1E7	17.8 (123)	11.1 (77)
1E8	15.9 (110)	9.9 (68)
1E9	14.2 (98)	8.8 (61)
1E10	12.6 (87)	7.9 (54)
1E11	11.2 (77)	7.0 (48)

GENERAL NOTES:
(a) All notes in Figures I-9.1 and I-9.1M apply to this data.
(b) Interpolation between tabular values is permissible based upon data representation by straight lines on log–log plot. see Table I-9.0 or Table I-9.0M, General Note (b).

NOTES:
(1) The number of cycles indicated shall be read as follows: IEJ = I × 10^J, e.g., 5E6 = 5 × 10^6 or 5,000,000
(2) These data points are included to provide accurate representation of curves at branches or cusps.

Figure 7.9 – Allowable alternating stress from ASME design fatigue curve for carbon steel and low alloy steel (ASME BPV Code, Section III, Mandatory Appendix I , Table I-9.1)

Table I-9.2
Tabulated Values of S_a, ksi (MPa), From Figures I-9.2 and I-9.2M

Number of Cycles [Note (1)]	Stress Amplitude
1E1	870 (6 000)
2E1	624 (4 300)
5E1	399 (2 748)
1E2	287 (1 978)
2E2	209 (1 440)
5E2	141 (974)
1E3	108 (745)
2E3	85.6 (590)
5E3	65.3 (450)
1E4	53.4 (368)
2E4	43.5 (300)
5E4	34.1 (235)
1E5	28.4 (196)
2E5	24.4 (168)
5E5	20.6 (142)
1E6	18.3 (126)
2E6	16.4 (113)
5E6	14.8 (102)
1E7	14.4 (99.0)
1E8	14.1 (97.1)
1E9	13.9 (95.8)
1E10	13.7 (94.4)
1E11	13.6 (93.7)

GENERAL NOTES:
(a) All notes in Figures I-9.2 and I-9.2M apply to this data.
(b) Interpolation between tabular values is permissible based upon data representation by straight lines on log–log plot. See Table I-9.0 or Table I-9.0M, General Note (b).

NOTE:
(1) The number of cycles indicated shall be read as follows: IEJ = I × 10^J, e.g., 5E6 = 5 × 10^6 or 5,000,000

Figure 7.10 – Allowable alternating stress from ASME design fatigue curve for austenitic steel (ASME BPV Code, Section III, Mandatory Appendix I, Table I-9.2)

Table NB-3681(a)-1
Stress Indices for Use With Equations in NB-3650

Piping Products and Joints [Note (3)]	Applicable for $D_o/t \le 100$ for C or K Indices and $D_o/t \le 50$ for B Indices [Note (1)]									Notes
	Internal Pressure [Note (2)]			Moment Loading [Note (2)]			Thermal Loading			
	B_1	C_1 [Note (4)]	K_1 [Note (4)]	B_2	C_2 [Note (4)]	K_2 [Note (4)]	C_3	C_3'	K_3 [Note (4)]	
Straight pipe, remote from welds or other discontinuities	0.5	1.0	1.0	1.0	1.0	1.0	0.6	0.5	1.0	(5)
Longitudinal butt welds in straight pipe										
(a) flush	0.5	1.0	1.1	1.0	1.0	1.1	1.0	...	1.1	(6)
(b) as-welded $t > 3/16$ in. (5 mm)	0.5	1.1	1.2	1.0	1.2	1.3	1.0	...	1.2	(6)
(c) as-welded $t \le 3/16$ in. (5 mm)	0.5	1.4	2.5	1.0	1.2	1.3	1.0	...	1.2	(6)
Girth butt welds between nominally identical wall thickness items										
(a) flush	0.5	1.0	1.1	1.0	1.0	1.1	0.60	0.50	1.1	(7)
(b) as-welded	0.5	1.0	1.2	1.0	...	1.8	0.60	0.50	1.7	(7)
Girth fillet weld to socket weld, fittings, socket weld valves, slip-on or socket welding flanges	...	...	3.0	...	...	2.0	2.0	1.0	3.0	(8)
NB-4250 transitions										
(a) flush	0.5	...	1.1	1.0	...	1.1	...	1.0	1.1	(9)
(b) as-welded	0.5	...	1.2	1.0	...	1.8	...	1.0	1.7	(9)
Transitions within a 1:3 slope envelope										
(a) flush	0.5	...	1.2	1.0	...	1.1	...	0.60	1.1	(10)
(b) as-welded	0.5	...	1.2	1.0	...	1.8	...	0.60	1.7	(10)
Butt welding reducers per ASME B16.9 or MSS SP-87	...	...	...	1.0	...	...	1.0	0.5	1.0	(11)
Curved pipe or butt welding elbows	...	...	1.0	...	...	1.0	1.0	0.5	1.0	(12)
Branch connections per NB-3643	0.5	...	2.0	...	...	...	1.8	1.0	1.7	(13)
Butt welding tees	0.5	1.5	4.0	...	...	...	1.0	0.5	1.0	(14)

GENERAL NOTE: For indices not listed, see the note referenced at the end of the applicable line.

NOTES:
(1) For products and joints with $50 < D_o/t \le 100$, see NB-3683.2(c).
(2) For the calculation of pressure and moment loads and special instructions regarding eqs. NB-3652(9) through NB-3653.6(b)(13), see NB-3683.1(d).
(3) For definitions, applicability, and specific restrictions, see NB-3683.
(4) For special instructions regarding the use of these indices for welded products, intersecting welds, abutting products, or out-of-round products, see NB-3683.2.
(5) See NB-3683.3, Straight Pipe Remote From Welds.
(6) See NB-3683.4(a), Longitudinal Butt Welds.
(7) See NB-3683.4(b), Girth Butt Welds.
(8) See NB-3683.4(c), Girth Fillet Welds.
(9) See NB-3683.5(a), NB-4250 Transitions.
(10) See NB-3683.5(b), Transitions Within a 1:3 Slope.
(11) See NB-3683.6, Concentric and Eccentric Reducers.
(12) See NB-3683.7, Curved Pipe or Butt Welding Elbows. See also NB-3683.2(a) and NB-3683.2(b).
(13) See NB-3683.8, Branch Connections per NB-3643. See also NB-3683.1(d).
(14) See NB-3683.9, Butt Welding Tees. See also NB-3683.1(d).

Figure 7.11 – Stress indices for ASME BPVC 2015 subsection NB (ASME BPV Code, Section III, Table NB-3681(a)-1)

Table 18-10 — Stress range $\Delta\sigma_R$ for $N \geq 2 \times 10^6$ cycles for unnotched test bars of ferritic and austenitic rolled and forged steels at room temperature and zero mean stress

Tensile strength R_m, MPa	Stress range at N cycles, MPa	
	$N = 2 \times 10^6$	$N = 10^8$
	$\Delta\sigma_D$	$\Delta\sigma_{Cut}$
400	273	184
600	399	270
800	525	355
1000	651	440

Figure 7.12 – Allowable alternating stress from EN design fatigue curve for unwelded components (SS-EN 13445, 2009, Part 3, Chapter 18, Table 18-10)

Table 18-4 — Class of weld details for use with structural equivalent stress range *(continued)*

a) Seam welds

Detail No.	Joint type	Sketch of detail	Comments	Class	
				Testing group 1 or 2	Testing group 3
1.5	Full penetration butt welds made from one side without backing		If full penetration can be assured*.	63	40
			If inside cannot be visually inspected and full penetration cannot be assured*.	40	40
1.6	Full penetration butt welds made from one side onto permanent backing.		Circumferential seams only (see 5.7) Minimum throat = shell thickness		
			Weld root pass inspected to ensure full fusion to backing.	56	40
			Single pass weld.	40	40
1.7	Joggle joint		Circumferential seams only (see 5.7) Minimum throat = shell thickness.		
			Weld root pass inspected to ensure full fusion to backing.	56	40
			Single pass weld.	40	40
*In case of misalignment, see 18.10.4.					

Figure 7.13 – Weld classes from EN for welded components (SS-EN 13445, Part 3, Chapter 18, Table 18-4)

Table 18-7 — Coefficients of the fatigue design curves for welded components

Class	Constants of $\Delta\sigma_R$ - N curve*				Stress range at N cycles, MPa	
	For $10^2 < N < 5x10^6$		For $5x10^6 < N < 10^8$		$N = 5 \times 10^6$	$N = 10^8$
	m_1	C_1	m_2	C_2	$\Delta\sigma_D$	$\Delta\sigma_{Cut}$
100	3,0	$2{,}00 \times 10^{12}$	5,0	$1{,}09 \times 10^{16}$	74	40
90	3,0	$1{,}46 \times 10^{12}$	5,0	$6{,}41 \times 10^{15}$	66	36
80	3,0	$1{,}02 \times 10^{12}$	5,0	$3{,}56 \times 10^{15}$	59	32
71	3,0	$7{,}16 \times 10^{11}$	5,0	$1{,}96 \times 10^{15}$	52	29
63	3,0	$5{,}00 \times 10^{11}$	5,0	$1{,}08 \times 10^{15}$	46	26
56	3,0	$3{,}51 \times 10^{11}$	5,0	$5{,}98 \times 10^{14}$	41	23
50	3,0	$2{,}50 \times 10^{11}$	5,0	$3{,}39 \times 10^{14}$	37	20
45	3,0	$1{,}82 \times 10^{11}$	5,0	$2{,}00 \times 10^{14}$	33	18
40	3,0	$1{,}28 \times 10^{11}$	5,0	$1{,}11 \times 10^{14}$	29,5	16
32	3,0	$6{,}55 \times 10^{10}$	5,0	$3{,}64 \times 10^{13}$	24	13
* For $E = 2{,}09 \times 10^5$ MPa						

Figure 7.14 – Allowable alternating stress from EN design fatigue curve for welded components (SS-EN 13445, Part 3, Chapter 18, Table 18-7)

Figure	Allowable half stress intensity range S_a [1)2)] at allowable number of load cycles $\hat{n}$																									
	$1{\cdot}10^1$	$2{\cdot}10^1$	$5{\cdot}10^1$	$1{\cdot}10^2$	$2{\cdot}10^2$	$5{\cdot}10^2$	$1{\cdot}10^3$	$2{\cdot}10^3$	$5{\cdot}10^3$	$1{\cdot}10^4$	$1.2{\cdot}10^{4*}$	$2{\cdot}10^4$	$5{\cdot}10^4$	$1{\cdot}10^5$	$2{\cdot}10^5$	$5{\cdot}10^5$	$1{\cdot}10^6$	$2{\cdot}10^6$	$5{\cdot}10^6$	$1{\cdot}10^7$	$2{\cdot}10^7$	$5{\cdot}10^7$	$1{\cdot}10^8$	$1{\cdot}10^9$	$1{\cdot}10^{10}$	$1{\cdot}10^{11}$
7.8-1: curve tensile strength 790 - 900 N/mm²	2900	2210	1590	1210	931	689	538	427	338	303	296	248	200	179	165	152	138									
7.8-1: curve tensile strength ≤ 550 N/mm²	4000	2830	1900	1410	1070	724	572	441	331	262	—	214	159	138	114	93.1	86.2									
7.8-2 T ≤ 80 °C	4341	3302	2312	1773	1368	981	770	612	461	378	—	316	257	225	201	178	165	156	147	142	138	135	133	129	128	127
7.8-2 T > 80 °C	4618	3467	2381	1798	1363	953	732	568	413	330	—	268	209	178	154	132	120	112	103	99	95	92	91	87	86	86
7.8-3	5508	3947	2522	1816	1322	894	684	542	413	338	—	275	216	180	154	130	116	104	94	91	—	—	89	88	87	86
7.8-4: curve maximum nominal stress [3)] ≤ 2.7 · S_m	7930	5240	3100	2210	1550	986	689	490	310	234	—	186	152	131	117	103	93.1									
7.8-4: curve maximum nominal stress [3)] = 3.0 · S_m	7930	5240	3100	2070	1415	842	560	380	230	155	—	105	73	58	49	42	36.5									

[1)] The values of S_a shown here are based on the respective elastic moduli of **Figures 7.8-1** to **7.8-4**.

[2)] Straight interpolation between tabular values is permitted based upon a double logarithmic representation: (straight lines between the data points on the log log plot). Where for a given value of $S_a = S$ the pertinent number of load cycles $\hat{n}$ is to be determined, this shall be done by means of the adjacent data points $S_j < S < S_i$ and $n_j > n > n_i$ as follows:

$$\hat{n} / \hat{n}_i = \left(\hat{n}_j / \hat{n}_i\right)^{\log\frac{S_i}{S} / \log\frac{S_i}{S_j}}$$

Example: Given: Steel with tensile strength ≤ 550 N/mm², $S_a = 370$ N/mm²

from which follows: $S_i = 441$ N/mm², $S_j = 331$ N/mm², $\hat{n}_i = 2 \cdot 10^3$, $\hat{n}_j = 5 \cdot 10^3$

$$\hat{n} / 2000 = (5000 / 2000)^{\log\frac{441}{370} / \log\frac{441}{331}}$$

$$\hat{n} = 3500$$

[3)] Nominal stress = tensile stress + bending stress

* This data point is included to provide accurate representation of the curve.

Table 7.8-3: Table of values for the design fatigue curves of Figures 7.8-1 to 7.8-4

Figure 7.15 – Allowable alternating stress from KTA design fatigue curves (KTA, Part 2, Table 7.8-3)

Description	Sketch	Shape factor h and configuration requirements [1]	Flexibility factor k (k ≥ 1) [2]	Stress intensification factor i (i ≥ 1) [3]	Section modulus [4]
1. Straight pipe		—	1	1	$\frac{\pi}{32} \cdot \frac{d_a^4 - d_i^4}{d_a}$
2. Welding elbow or pipe bend [5]	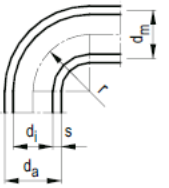	$\frac{4 \cdot r \cdot s}{d_m^2}$	$\frac{1.65}{h}$	$\frac{0.9}{h^{2/3}}$	
6. Butt weld	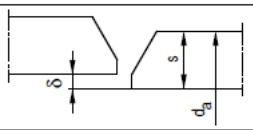	s ≥ 5 mm and δ ≤ 0.1·s	1	1.0	$\frac{\pi}{32} \cdot \frac{d_a^4 - d_i^4}{d_a}$
		s < 5 mm or δ > 0.1·s	1	flush: 1.0 as-welded: 1.8	

Table 8.5-5: Flexibility characteristics and factors, stress intensification factors and section moduli

Figure 7.16 – Stress intensification factors from KTA code (KTA, Part 2, Table 8.5-5)

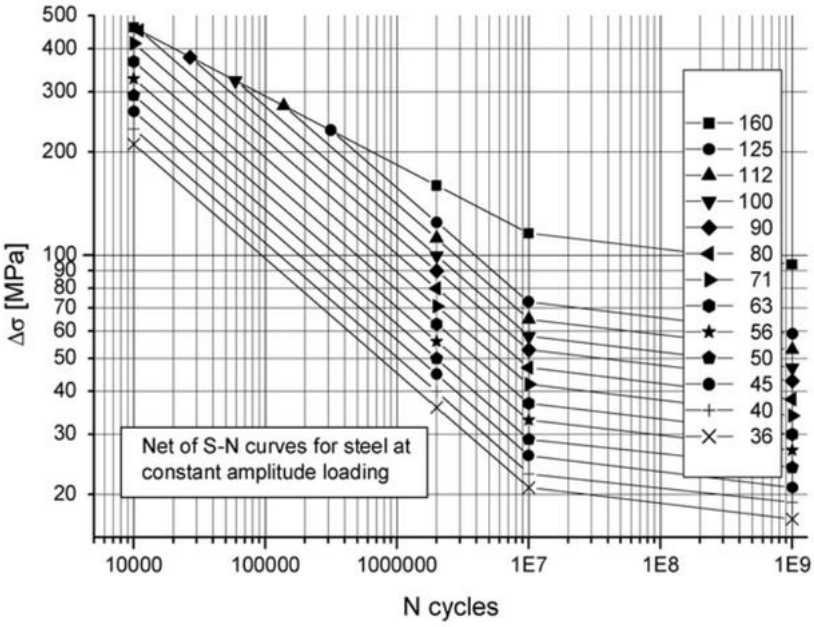

Figure (3.2)-2: Fatigue resistance S-N curves for steel, normal stress, very high cycles applications

Figure 7.17 – Design fatigue curves for welded components from IIW code (IIW, Figure(3.2)-2)

No.	Structural Detail	Description (St.= steel; Al.= aluminium)	FAT St.	FAT Al.	Requirements and Remarks
226	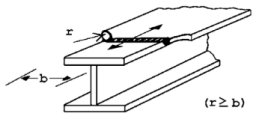	Transverse butt weld flange splice in built-up section welded prior to the assembly, ground flush, with radius transition, NDT	100	40	All welds ground flush to surface, grinding parallel to direction of stress. Weld run-on and run-off pieces to be used and subsequently removed. Plate edges ground flush in direction of stress.
231	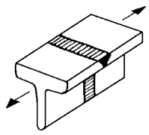	Transverse butt weld splice in rolled section or bar besides flats, ground flush, NDT	80	28	All welds ground flush to surface, grinding parallel to direction of stress. Weld run-on and run-off pieces to be used and subsequently removed. Plate edges ground flush in direction of stress.
232	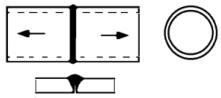	Transverse butt weld splice in circular hollow section, welded from one side, full penetration, potential failure from root . root inspected by NDT no NDT	 71 36	 28 12	Welded in flat position. Axial misalignment < 5% of wall thickness

Figure 7.18 - FAT classes from IIW for transversely loaded butt weld in pipe component (IIW, Tab. {3.2}-1)

Appendix D Elements

The ANSYS Workbench element library there is a number of different element options to choose from. The elements are classified into groups based on spatial dimension. These groups of elements contain element name, physical property and element type. In ANSYS these element groups are characterized as: 0D elements (mass elements), 1D elements (beam - and spring-damper elements), 2D elements (shell elements), 3D elements (solid- and solid/shell elements) and contact elements.

7.1.1.1 SOLSH190 elements

SOLSH190 element is used for simulation of shell structures with a range of thicknesses, from very thin to moderately thick (ANSYS 2019, chapter 7: element library). The SOLSH190 element has 8 nodes with 3 translational DOF at each node: translation in x,y and z-directions (ANSYS 2019, chapter 7: element library). Linear interpolation is used to determine the element behaviour and element orientation normal to the mid-surface (Banerjee, B. et.al., 2013).
In SOLSH190 5 integration points are used through the thickness (Wang, E, 2006). Illustration of the SOLSH190 is provided in Figure 7.19.

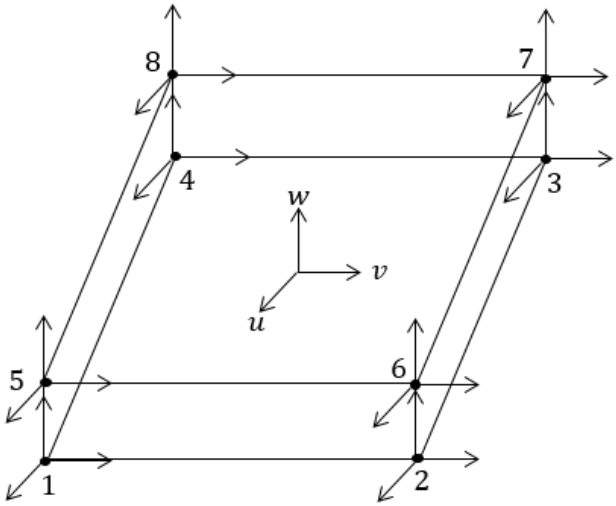

Figure 7.19- SOLSH190 element with 3 translational DOF in node 1-8

7.1.1.2 COMBIN14 elements

COMBIN14 elements have longitudinal and torsional capabilities in 1D, 2D or 3D applications (ANSYS manual, 2019). COMBIN14 element has two options: longitudinal spring-damper option and torsional spring-damper option. Longitudinal spring-damper option is a uniaxial tension-compression element with 3 DOF in every node, translations in x, y and z-directions. The torsional spring-damper option is a pure rotational element with 3 DOF in every node, rotations in x, y and z-directions. The spring-damper element is considered to be idealized, i.e. the spring is considered to be massless. Mass can be included by incorporating an appropriate mass element. In ANSYS it is possible to deactivate damping and only specify spring stiffness and compression loads. COMBIN14 geometry is depicted in Figure 7.20.

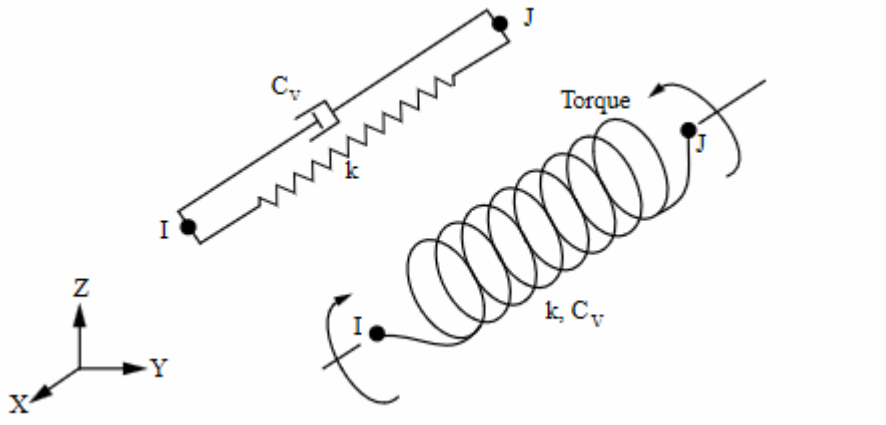

Figure 7.20 - COMBIN14 element geometry with notations (ANSYS 2019, chapter 7: element library)

I and J represents the nodes, k is the spring constant, C_v is the damping coefficient (neglected in this thesis) and the arrows denote rotation around the x-axis. For a 3D element there is two additional DOF, rotation around the y and z-axis.

7.1.1.3 CONTA175 & TARGE170 elements

CONTA175 is an element used to represent contact or sliding between a node and a surface in 2D or 3D. In a 3D element every node contains 3 DOF displacements in x,y and z-directions. The element is intended for rigid-flexible and flexible-flexible contacts (ANSYS, 2019). CONTA175 determines contact and potential sliding between surfaces and a contact pair is created (Malekova, V., Jendzelovsky. 2012), illustrated in Figure 7.21.

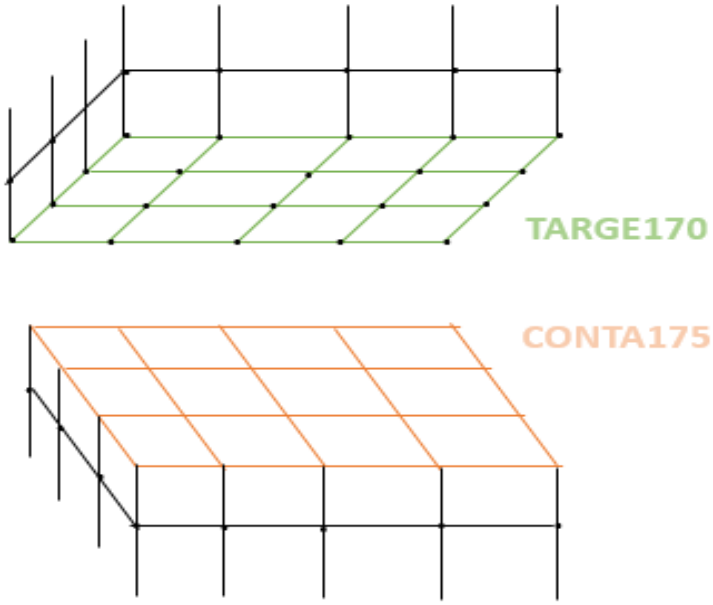

Figure 7.21- Definition of a contact pair

In the case of general contact, the target surface can be defined by CONTA175 or TARGE170 elements, CONTA175 is for deformable bodies and TARGE170 is limited to rigid bodies (ANSYS 2019, chapter 7: element library). TARGE170 elements are used to

represent 3D target surfaces for the associated contact element. The contact element overlaps the solid shell element edges which describes the boundary of a deformable body in contact with the rigid target surface, defined by TARGE170. A target can be described as a three-dimensional geometric entity that senses and responds when a contact element moves into a target surface element.

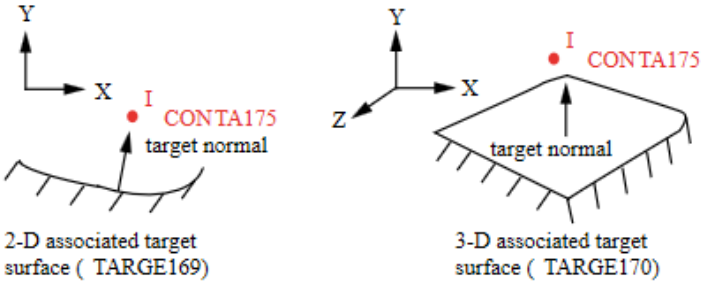

Figure 7.22- CONTA175 element and surface TARGE170 element (ANSYS 2019, chapter 7: element library)

7.1.1.4 MASS21 elements

MASS21 is a point element containing 6 DOF: translations in x,y- and z-directions and rotations around the nodal in x,y- and z-axes (ANSYS 2019, chapter 7: element library). MASS21 element is defined by a single node with mass components in the element directions $\left(\frac{Force \times Time^2}{Length}\right)$ and rotation inertia ($Force \times Length \times Time^2$) about the element coordinate axes (ANSYS 2019, chapter 7: element library). The MASS21 geometry is depicted in Figure 7.23.

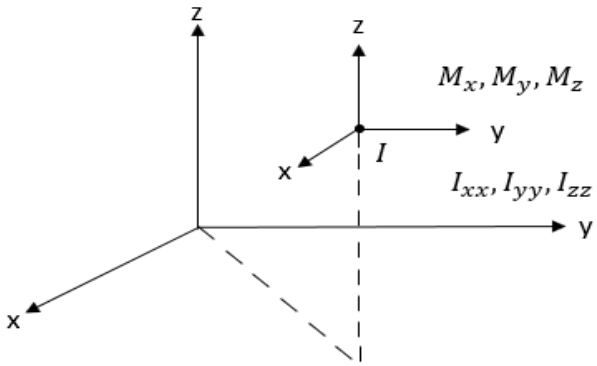

Figure 7.23 - MASS21 geometry

Where M_x, M_y, M_z represent concentrated mass components in x, y and z-directions and I_{xx}, I_{yy}, I_{zz} represent the rotation inertia around the x, y and z-axes.

Appendix E MATLAB Code

D.1 ASME function

```
function [v_allow_FEM, v_allow_analytic] = ASME_OM(Sel,C1,C3,C4,C5,C2K2,alpha,beta,f,maxU,maxS)
% ASME_OM calculate allowable vibration velocity according to velocity
% method in ASME OM-2015.
maxV = maxU*2*pi.*f; % Calculate maximum velocity of harmonic signal from signal amplitude.
K = maxS./maxV; % Susceptibility factor as defined in ASME OM-2015.
v_allow_analytic = (C1*C4*beta*(Sel/1e6)./(C3*C5*alpha.*C2K2))/sqrt(2); % rms value in mm/s
v_allow_FEM = (Sel./(C2K2.*alpha.*K)).*1000./sqrt(2); % rms value in mm/s
end
```

D.2 EN 13445 function

```
function [v_allow] = SS_EN(Sa,f,maxU,maxS)
% SS-EN-13445-3 calculate allowable vibration velocity from modal
% deflection by scaling Sa to match normal stress.
scaleFactor = maxS./Sa;
v_allow = (maxU./scaleFactor).*2.*pi.*f.*1000./sqrt(2);
end
```

D.3 VDI function

```
function [v_allow] = VDI(Sa,fm,fphi,fi,Do,E,I,mu)
% VDI3842 calculate allowable vibration velocity according to analytic
% method in VDI3842.
v_allow = Sa./(fm.*fphi.*fi.*Do.*0.5.*sqrt(E.*mu./I)).*1000./sqrt(2);
end
```

D.4 IIW function

```
function [v_allow] = IIW(Sa,f,maxU,maxS)
% IIW calculate allowable vibration velocity from modal
% deflection by scaling Sa to match normal stress.
scaleFactor = maxS./Sa;
v_allow = (maxU./scaleFactor).*2.*pi.*f.*1000./sqrt(2);
end
```

D.5 ASME C1 function

```
function [C1] = ASME_C1(m_konc,mu,cl)
% Calculate C1 concentrated mass correction factor for ASME
analytic method
m_ratio = m_konc./(mu*cl);
Kvot = [0% Ratio of concentrated weight to span weight
1 2 3 4 5 6 7 8 9 10 11 12 13 14 15 16 17 18 19 20 21 22 23 24
25];
C = [1% Correction factor dependent on ratio of concentrated
weight to span weight
0.500 0.390 0.340 0.300 0.260 0.230 0.210 0.200 0.190 0.185
0.180 0.175 0.170 0.165 0.160 0.155 0.150 0.145 0.140 0.135
0.130 0.125 0.120 0.115 0.110];
C1 = zeros(length(m_ratio),1);
for j=1:length(m_ratio)
    if m_ratio(j) == Kvot(1)
        C1(j) = C(1);
    elseif m_ratio(j) >= Kvot(end)
        x = [Kvot(end-1),Kvot(end)];
        v = [C(end-1), C(end)];
        xq = m_ratio(j);
        C1(j) = interp1(x,v,xq,'linear','extrap');
        if C1(j) < 0
            error('C1 coefficient is negative, ratio of
concentrated weight to span weight is undefined for
extrapolation')
        end
    else
        for i = 2:length(Kvot)   % Find interval m_ratio lies
between and linear interpolation to find exact value
            if m_ratio(j) < Kvot(i)
                x = [Kvot(i-1),Kvot(i)];
                v = [C(i-1),C(i)];
                xq = m_ratio(j);
                C1(j) = interp1(x,v,xq);
                break
            end
        end
    end
end
end
```

D.6 VDI fm function

```
function [fm] = VDI_fm(m_konc,mu,cl)
% VDI calculate concentrated mass correction factor fm from
graph in VDI.
% Interpolation between read values is implemented.
% For fixed ends of the three lines in VDI graph.
m_ratio = m_konc./(mu*cl);
Kvot = 0:0.5:10; % Ratio of concentrated weight to span weight
```

```
C = [1 1.2 1.4 1.55 1.8 1.95 2.2 2.3 2.35 2.45 2.5 2.55 2.65
2.7  2.8  2.85  2.9  2.98  3  3.05  3.1];% Correction factor
dependent on ratio of concentrated weight to span weight
fm = zeros(length(m_ratio),1);
for j=1:length(m_ratio)
    if m_ratio(j) == Kvot(1)
        fm(j) = C(1);
    elseif m_ratio(j) >= Kvot(end)
        x = [Kvot(end-1),Kvot(end)];
        v = [C(end-1), C(end)];
        xq = m_ratio(j);
        fm(j) = interp1(x,v,xq,'linear','extrap');
        if fm(j) < 0
            error('fm  coefficient  is  negative,  ratio  of
concentrated  weight  to  span  weight  is  undefined  for
extrapolation')
        end
        warning('Ratio  of  concentrated  weight  to  span  weight
is  out  of  bounds  for  VDI  graph.  Will  extrapolate  but  fm  can
reach infinity')
    else
        for  i  =  2:length(Kvot)   % Find interval m_ratio lies
between and linear interpolation to find exact value
            if m_ratio(j) < Kvot(i)
                x = [Kvot(i-1),Kvot(i)];
                v = [C(i-1),C(i)];
                xq = m_ratio(j);
                fm(j) = interp1(x,v,xq);
                break
            end
        end
    end
end
end
```